ORGANOMETALLICS

pubs.acs.org/Organometallics Article

Group 10 Metal Dithiolene Bis(isonitrile) Complexes: Synthesis, Structures, Properties, and Reactivity

Antony Obanda, Kendra Valerius, Joel T. Mague, Stephen Sproules, and James P. Donahue*

Cite This: *Organometallics* 2020, 39, 2854–2870 Read Online

ACCESS | Metrics & More | Article Recommendations | Supporting Information

ABSTRACT: The reaction of $[(Ph_2C_2S_2)_2M]$ (M = Ni^{2+}, Pd^{2+}, Pt^{2+}) with 2 equiv of RN≡C (R = Me (**a**), Bn (**b**), Cy (**c**), ^{t}Bu (**d**), 1-Ad (**e**), Ph (**f**)) yields $[(Ph_2C_2S_2)M(C{\equiv}NR)_2]$ (M = Ni^{2+}, **4a–f**; M = Pd^{2+}, **5a–f**; M = Pt^{2+}, **6a–f**), which are air-stable and amenable to chromatographic purification. All members have been characterized crystallographically. Structurally, progressively greater planarity tends to be manifested as M varies from Ni to Pt, and a modest decrease in the C≡N bond length of coordinated C≡NR appears in moving from Ni toward Pt. Vibrational spectroscopy (CH_2Cl_2 solution) reveals $\nu_{C{\equiv}N}$ frequencies for $[(Ph_2C_2S_2)M(C{\equiv}NR)_2]$ that are substantially higher than those for free C≡NR and increase as M ranges from Ni to Pt. This trend is interpreted as arising from an increasingly positive charge at M that stabilizes the linear, charge-separated resonance form of the ligand over the bent form with lowered C–N bond order. UV–vis spectra reveal lowest energy transitions that are assigned as HOMO (dithiolene π) → LUMO (M–L σ^*) excitations. One-electron oxidations of $[(Ph_2C_2S_2)M(C{\equiv}NR)_2]$ are observed at ∼+0.5 V due to $Ph_2C_2S_2^{2-}$ → $Ph_2C_2S^{-}S^{\bullet}$ + e^-. Chemical oxidation of $[(Ph_2C_2S_2)Pt(C{\equiv}N^tBu)_2]$ with $[(Br\text{-}p\text{-}C_6H_4)_3N][SbCl_6]$ yields $[(Ph_2C_2S^{-}S^{\bullet})Pt(C{\equiv}N^tBu)_2]^+$, identified spectroscopically, but in the crystalline state $[[(Ph_2C_2S^{-}S^{\bullet})Pt(C{\equiv}N^tBu)_2]_2]^{2+}$ prevails, which forms via axial Pt···S interactions and pyramidalization at the metal. Complete substitution of MeNC from $[(Ph_2C_2S_2)Ni(C{\equiv}NMe)_2]$ by 2,6-Me_2py under forcing conditions yields $[(2,6\text{-}Me_2py)Ni(\mu_2\text{-}\eta^1,\eta^1\text{-}S',\eta^1\text{-}S''\text{-}S_2C_2Ph_2)]_2$ (**8**), which features a folded Ni_2S_2 core. In most cases, isocyanide substitution from $[(Ph_2C_2S_2)M(C{\equiv}NMe)_2]$ with monodentate ligands (L = phosphine, CN^-, carbene) leads to $[(Ph_2C_2S_2)M(L)(C{\equiv}NMe)]^n$ (n = 0, 1−), wherein $\nu_{C{\equiv}N}$ varies according to the relative σ-donating power of L (**9–21**). The use of 1,3-bis(2,6-diisopropylphenyl)imidazol-2-ylidene (IPr) provides $[(Ph_2C_2S_2)M(IPr)(C{\equiv}NMe)]$ for M = Ni (**18**), Pd (**19**), but for Pt, attack by IPr at the isocyanide carbon occurs to yield the unusual η^1,κC-ketenimine complex $[(Ph_2C_2S_2)Pt(C(NMe)(IPr))(C{\equiv}NMe)]$ (**20**).

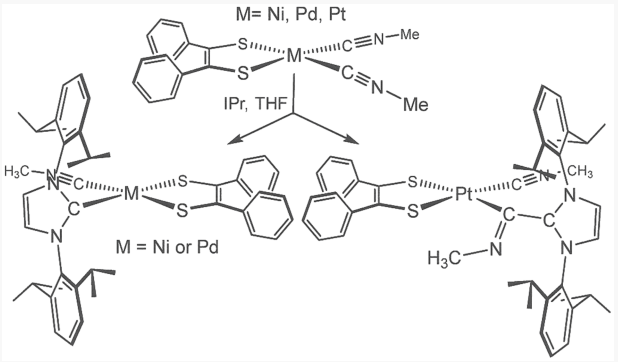

INTRODUCTION

In their charge-neutral state, the bis(dithiolene) complexes of the Group 10 metals are diamagnetic species comprised of a divalent metal ion and two dithiolene ligands in a radical monoanionic state, a redox level intermediate between fully reduced ene-1,2-dithiolate and fully oxidized α-dithione or dithiete (Scheme 1). In the presence of a suitable reacting partner, these complexes undergo a ligand redox disproportionation whereby one of the two dithiolene ligands is extruded or transferred in an oxidized form and the other ligand remains coordinated to M^{2+} as a dithiolate dianion (Scheme 2). As shown, Scheme 2 is a conceptual formalism representing a partitioning of electrons that accounts for the observed products, as opposed to being a discrete reaction step itself. This ligand redox disproportionation admits of two different perspectives. On one hand, $[(R_2C_2S_2)_2M]$ complexes effectively operate as delivery agents of reactive oxidized dithiolene ligands that are otherwise not isolable and that can oxidatively add to a low-valent coordination complex, if present. The original and historically important example of this reactivity was synthesis by Schrauzer of $[(R_2C_2S_2)_2M(CO)_2]$ (M = Mo, W; R = Ph, Me).[1] These molecules have been of considerable usefulness as entry points toward small-molecule analogues of the catalytic sites of molybdo- and tungstoenzymes.[2] Others,[3−8] particularly Morris and co-workers,[4−8] have effectively exploited this behavior for the preparation of a variety of new organometallic and inorganic transition-metal complexes. In these examples, the value-added product is the coordination complex formed by oxidative addition of the dithiolene ligand, while $[(R_2C_2S_2)M]_x$ is separated as an

Received: June 1, 2020
Published: July 30, 2020

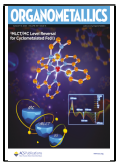

https://dx.doi.org/10.1021/acs.organomet.0c00375
Organometallics 2020, 39, 2854–2870

Scheme 1. Redox Levels of a Dithiolene Ligand

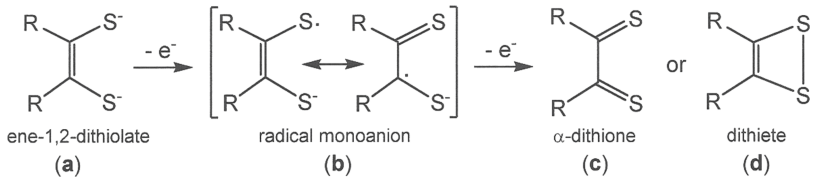

Scheme 2. Dithiolene Ligand Redox Disproportionation in Group 10 Bis(dithiolene) Complexes[a]

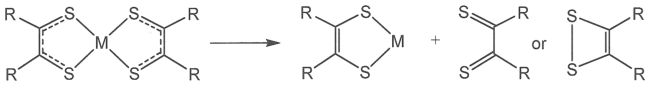

[a]This scheme is a formalism that rationalizes products formed in reactions with other metal complexes and is not a depiction of a discrete reaction.

oligomeric or insoluble polymeric byproduct. On the other hand, if a suitable ligand L is introduced to $[(R_2C_2S_2)_2M]$, well-defined new heteroleptic dithiolene complexes of the form $[(R_2C_2S_2)ML_2]$ (L_2 = two monodentate or one bidentate soft σ-donor) are efficiently produced, while the expelled oxidized dithiolene ligand is separated as an ill-defined oligomer or polymer. Here again, the original example of this reaction type was described by Schrauzer, who found it to be a direct and effective route toward $[(R_2C_2S_2)M(PR_3)_2]$ complexes.[1,9]

As detailed in a recent account,[10] we were motivated to survey the generality of dithiolene extrusion from $[(R_2C_2S_2)_2M]$ to form $[(R_2C_2S_2)ML_2]$ beyond the limited bounds of Schrauzer's work because of the potential we saw for the use of $[(R_2C_2S_2)ML_2]$ compounds in the targeted synthesis of complex multimetal dithiolene complexes. The syntheses of $[(Ph_2C_2S_2)M(CNR)_2]$ (M = Ni^{2+}, Pd^{2+}, Pt^{2+}; R = Me, Cy, ^{t}Bu, 1-Ad, Ph) were disclosed in that report as well as a preliminary study of the further reactivity of $[(Ph_2C_2S_2)Ni(CNMe)_2]$. In this following work, we more fully characterize the $[(Ph_2C_2S_2)M(CNR)_2]$ compounds, especially structurally, and we more thoroughly lay out the panorama of outcomes when $[(Ph_2C_2S_2)M(CNMe)_2]$ (M = Ni^{2+}, Pd^{2+}, Pt^{2+}) are introduced to new ligands intended to substitute for MeNC.

EXPERIMENTAL SECTION

Physical Methods. UV−vis spectra were obtained at ambient temperature with a Hewlett-Packard 8455a diode array spectrometer, while IR spectra were taken as CH_2Cl_2 solutions with a Thermo Nicolet Nexus 670 Fourier transform infrared instrument in absorption mode. All ^{1}H, ^{13}C, and ^{31}P NMR spectra were recorded at 25 °C with a Varian Unity Inova spectrometer operating at 400 MHz or with a Bruker Avance spectrometer operating at 300 MHz. Both ^{1}H and ^{13}C NMR spectra were referenced to the solvent signal, while an external aqueous H_3PO_4 solution was employed as a reference for all ^{31}P spectra. X-band EPR spectra were recorded on a Bruker ELEXSYS E500 spectrometer, while simulations were performed with XSophe[11] distributed by Bruker Biospin GmbH. Mass spectra (MALDI-TOF, matrix-assisted laser desorption ionization−time of flight) were obtained with a Bruker Autoflex III instrument operating in positive ion mode. Electrochemical measurements were made with a CHI 620C electroanalyzer workstation using a Ag/AgCl reference electrode, a glassy-carbon-disk working electrode, a Pt-wire auxiliary electrode, and $[^nBu_4N][PF_6]$ as the supporting electrolyte. Typical scan rates were 50 and 100 mV/s. Under these conditions, the Cp_2Fe^+/Cp_2Fe couple consistently occurred at +540 mV. Elemental analyses were performed by Midwest Microlab, LLC (Indianapolis, IN), Galbraith Laboratories, Inc. (Knoxville, TN), or Kolbe Microanalytical Laboratory (Oberhausen, Germany). Details regarding the collection of X-ray diffraction data and the solution and refinement of crystal structures are given in the Supporting Information.

Syntheses. The $[(Ph_2C_2S_2)_2M]$ (M = Ni^{2+}, Pd^{2+}, Pt^{2+}) starting materials were synthesized following the procedure outlined by Schrauzer and Mayweg.[1] Methyl isocyanide was made by the dehydration of *N*-methylformamide,[12] and its density was experimentally determined to be 0.78 g/mL, while *tert*-butyl isocyanide (d = 0.74 g/mL) and phenyl isocyanide (d = 0.98 g/mL)[13] were synthesized via the phase-transfer Hofmann-carbylamine reaction.[14] Cyclohexyl isocyanide (d = 0.878 g/mL), 1-adamantyl isocyanide, benzyl isocyanide (d = 0.962 g/mL), and $[Et_4N][CN]$ were used as received from commercial sources. Tetraisopropylbenzobisimidazolium dibromide was prepared following a published procedure[15] and deprotected by a modification of the protocol by Bantreil and Nolan.[16] The $[BF_4]^-$ salt of $[IPr\text{-}H]^+$ (IPr = 1,3-bis(2,6-diisopropylphenyl)imidazol-2-ylidene) was prepared and unmasked under N_2 following the same protocol reported by Bantreil and Nolan.[16] The free IPr ligand was stored in a glovebox. A published procedure was also implemented for the synthesis of *p*-phenylenebis(diphenylphosphine) (1,4-dppb).[17] Column chromatography separations were carried out using 63−200 μm silica (Dynamic Adsorbents) or 150 mesh neutral alumina (Aldrich). The solvents used for reactions were either dried with a system of drying columns from the Glass Contour Company (CH_2Cl_2, THF), freshly distilled according to standard procedures[18] (MeCN), or used as received from commercial suppliers. All reactions were conducted under an inert atmosphere of either N_2 or Ar. Subsequent purification by chromatography and crystallization were done in the open air, except where noted otherwise.

$[(Ph_2C_2S_2)Ni(CNBn)_2]$ (4b). Benzyl isocyanide (0.040 mL, 0.33 mmol) was delivered dropwise via a gastight syringe to a solution of $[(Ph_2C_2S_2)_2Ni]$ (0.100 g, 0.184 mmol) in CH_2Cl_2 (20 mL). The mixture was stirred at 25 °C for 5 h, after which time the solvent was removed under reduced pressure. The dark blue solid residue was applied directly to the top of a silica gel column packed as a slurry in hexanes. Flash elution with 1/1 CH_2Cl_2/hexanes moved a green band of unreacted $[(Ph_2C_2S_2)_2Ni]$ followed by a well-resolved blue band of **4b**. This blue fraction was collected using 2/1 CH_2Cl_2/hexanes and taken to dryness under reduced pressure. The solid residue was washed with *n*-pentane (5 mL), redissolved in a minimal volume of CH_2Cl_2, filtered through a Celite pad, and taken to dryness again. Crystallization was accomplished by slow diffusion of hexanes vapor into a concentrated 1,2-dichloroethane solution. Yield: 0.089 g, 91%. R_f = 0.39 (2/1 CH_2Cl_2/hexanes). ^{1}H NMR (δ, ppm in CD_2Cl_2): 7.46−7.35 (overlapping m, 10H, Bn aromatic C−*H*), 7.19−7.09 (overlapping m, 10H, aromatic C−*H*), 4.88 (s, 4H, C*H*$_2$). ^{13}C NMR (δ, ppm in CD_2Cl_2): 142.1, 138.6, 131.7, 130.1, 129.6, 129.3, 128.0, 127.2, 126.5, 48.7 (CH_2). IR (CH_2Cl_2, cm^{-1}): 2213 (vs, CN_{sym}), 2197 (vs, CN_{asym}). UV−vis absorption spectrum [CH_2Cl_2, λ_{max}, nm (ε_M, M^{-1} cm^{-1})]: 460 (400), 608 (420). Cyclic voltammetry (CV): **4b** − e^- → $[\mathbf{4b}]^+$, +0.50 V. Anal. Calcd for $C_{30}H_{24}N_2S_2Ni$: C, 67.31; H, 4.52; N, 5.23. Found: C, 67.18; H, 4.67; N, 5.21.

$[(Ph_2C_2S_2)Ni(CNCy)_2]$ (4c). The same procedures and scale used in the synthesis of **4b** were employed but with 0.05 mL (0.40 mmol) of cyclohexyl isocyanide. Ultimately, dark purple crystals of **4c** were obtained. Yield: 0.082 g, 95%. R_f = 0.52 (2/1 CH_2Cl_2/hexanes). ^{1}H NMR (δ, ppm in CD_2Cl_2): 7.17−7.08 (overlapping m, 10H, aromatic C−*H*), 3.90 (m, 2H, Cy −C*H*NC), 1.94−1.89 (m, 4H, Cy), 1.81−

https://dx.doi.org/10.1021/acs.organomet.0c00375
Organometallics 2020, 39, 2854−2870

1.73 (m, 8H, Cy), 1.54−1.46 (m, 8H, Cy). ^{13}C NMR (δ, ppm in CD_2Cl_2): 142.4, 138.4, 135.9 (t), 130.1, 127.9, 126.3, 55.4 (Cy, *C*H), 32.4 (Cy, CH_2), 25.2 (Cy, CH_2), 22.9 (Cy, CH_2). IR (CH_2Cl_2, cm^{-1}): 2204 (vs, CN_{sym}), 2189 (vs, CN_{asym}). UV−vis absorption spectrum (CH_2Cl_2, λ_{max}, nm (ε_M, M^{-1} cm^{-1})): 440 (240), 601 (420). MALDI MS: calcd for $C_{28}H_{32}N_2S_2Ni$ *m*/*z* 519.401; obsd *m*/*z* 519.042. Cyclic voltammetry: **4c** − e^- → $[\mathbf{4c}]^+$, +0.56 V. Anal. Calcd for $C_{28}H_{32}N_2S_2Ni$: C, 64.74; H, 6.22; N, 5.39. Found: C, 64.86; H, 5.95; N, 5.43.

[($Ph_2C_2S_2$)Ni(CN^tBu)$_2$] (4ad). A 0.040 mL portion (0.36 mmol) of *tert*-butyl isocyanide was delivered dropwise via a gastight syringe to a solution of **1a** (0.100 g, 0.184 mmol), in CH_2Cl_2 (25 mL) under an Ar atmosphere. Subsequent workup and purification were as described for **4b**. Crystallization was accomplished by slow diffusion of Et_2O vapor into a concentrated CH_2Cl_2 solution to ultimately give dark blue crystals of **4ad**. Yield: 0.067 g, 81%. R_f = 0.46 (2/1 CH_2Cl_2/hexanes). ^{1}H NMR (δ, ppm in CD_2Cl_2): 7.16−7.14 (m, 4H, aromatic C−*H*), 7.12−7.09 (m, 6H, aromatic C−*H*), 1.53 (s, 18H, ^{t}Bu). ^{13}C NMR (δ, ppm in CD_2Cl_2): 141.8, 138.0, 135.1 (t), 129.9, 127.6, 126.0, 58.3 (t, ^{t}Bu *tert*-*C*), 30.4 (^{t}Bu *C*H$_3$). IR (CH_2Cl_2, cm^{-1}): 2197 (vs, CN_{sym}), 2180 (vs, CN_{asym}). UV−vis absorption spectrum [CH_2Cl_2, λ_{max}, nm (ε_M, M^{-1} cm^{-1})]: ∼424 (260), 600 (410). Cyclic voltammetry: **4ad** − e^- → $[\mathbf{4ad}]^+$, +0.59 V. Anal. Calcd for $C_{24}H_{28}N_2S_2Ni$: C, 61.68; H, 6.04; N, 5.99. Found: C, 61.91; H, 6.04; N, 6.08.

[((MeO-*p*-C_6H_4)$_2C_2S_2$)Ni(CN^tBu)$_2$] (4bd). A portion of *tert*-butylisocyanide (0.03 mL, 0.27 mmol) amounting to two equiv was added via syringe to a solution of [((MeO-*p*-C_6H_4)$_2C_2S_2$)$_2$Ni] (0.100 g, 0.151 mmol) in CH_2Cl_2 (25 mL). Subsequent steps in workup and purification were analogous to those described for compound **4b**; dark blue crystals of **4bd** were ultimately obtained. Yield: 0.069 g, 98%. R_f = 0.37 (2/1 CH_2Cl_2/hexanes). ^{1}H NMR (δ, ppm in CD_2Cl_2): 7.11−7.06 (m, 2H, aromatic C−*H*), 6.69−6.64 (m, 2H, aromatic C−*H*), 3.73 (s, 6H, −O*CH*$_3$), 1.53 (s, 18H, ^{t}Bu). ^{13}C NMR (δ, ppm in $CDCl_3$): 157.9, 136.8, 134.9, 131.1, 113.1, 58.2 (^{t}Bu *tert*-*C*), 55.3 (−O*CH*$_3$), 30.3 (^{t}Bu *C*H$_3$). IR (CH_2Cl_2, cm^{-1}): 2196 (vs, CN_{sym}), 2180 (vs, CN_{asym}). UV−vis absorption spectrum [CH_2Cl_2, λ_{max}, nm (ε_M, M^{-1} cm^{-1})]: 420 (200), 607 (320). MALDI MS: calcd for $C_{26}H_{32}N_2O_2S_2Ni$ *m*/*z* 527.378, obsd *m*/*z* 527.071. Cyclic voltammetry: **4bd** − e^- → $[\mathbf{4bd}]^+$, +0.50 V. Anal. Calcd for $C_{26}H_{32}N_2O_2S_2Ni$: C, 59.21; H, 6.13; N, 5.31; S, 12.16. Found: C, 59.06; H, 6.05; N, 5.36; S, 12.01.

[($Me_2C_2S_2$)Ni(CN^tBu)$_2$] (4cd). Neat *tert*-butyl isocyanide (0.19 mL, 1.70 mmol) was delivered via syringe to a solution of [($Me_2C_2S_2$)$_2$Ni] (0.251 g, 0.85 mmol) in CH_2Cl_2 (25 mL). The remaining synthesis and purification steps were analogous to those employed for compound **4b**. Crystallization was achieved by diffusing hexanes into a concentrated toluene solution of **4cd** with a few drops of *tert*-butyl isocyanide placed in the inner vial. Yield: 0.086 g, 30%. R_f = 0.37 (2/1 CH_2Cl_2/hexanes). ^{1}H NMR (δ, ppm in CD_2Cl_2): 1.95 (s, 6H, −*CH*$_3$), 1.50 (s, 18H, ^{t}Bu). ^{13}C NMR (δ, ppm in $CDCl_3$): 135.8, 130.6, 58.4 (^{t}Bu *tert*-*C*), 30.4 (isocyanide −*CH*$_3$), 20.7 (dithiolene −*CH*$_3$). IR (CH_2Cl_2, cm^{-1}): 2196 (vs, CN_{sym}), 2177 (vs, CN_{asym}). UV−vis absorption spectrum [CH_2Cl_2, λ_{max}, nm (ε_M, M^{-1} cm^{-1})]: 350 (6400), 450 (290), 614 (170). Cyclic voltammetry: **4cd** − e^- → $[\mathbf{4cd}]^+$, +0.42 V.

[($Ph_2C_2S_2$)Ni(CN-1-Ad)$_2$] (4e). Solid 1-adamantyl isocyanide (0.054 g, 0.331 mmol) was added to a solution of **1** (0.090 g, 0.166 mmol) in CH_2Cl_2 (25 mL). Subsequent steps in the workup and purification procedure were similar to those implemented for **4b**, ultimately yielding dark blue crystals of **4e**. Yield: 0.076 g, 74%. R_f = 0.64 (2/1 CH_2Cl_2/hexanes). ^{1}H NMR (δ, ppm in CD_2Cl_2): 7.16−7.08 (overlapping m, 10H, aromatic C−*H*), 2.13 (m, 6H, admantyl C−*H*), 2.10 (m, 12H, adamantyl C−*H*), 1.70 (m, 12H, adamantyl C−*H*). ^{13}C NMR (δ, ppm in CD_2Cl_2): 142.4, 138.4, 134.5 (t), 130.1, 127.9, 126.3, 58.6, 43.3, 35.6, 29.3. IR (CH_2Cl_2, cm^{-1}): 2196 (vs, CN_{sym}), 2175 (vs, CN_{asym}). UV−vis absorption spectrum [CH_2Cl_2, λ_{max}, nm (ε_M, M^{-1} cm^{-1})]: 437 (180), 599 (360). Cyclic voltammetry: **4e** − e^- → $[\mathbf{4e}]^+$, +0.57 V. Anal. Calcd for $C_{36}H_{40}N_2S_2Ni$: C, 69.34; H, 6.47; N, 4.49. Found: C, 69.22; H, 6.33; N, 4.54.

[($Ph_2C_2S_2$)Ni($CNPh$)$_2$] (4f). The procedure followed for the synthesis of **4b** was employed using 0.080 mL (0.76 mmol) of phenyl isocyanide, which was added to a solution of [($Ph_2C_2S_2$)$_2$Ni] (0.220 g, 0.405 mmol) in CH_2Cl_2 (25 mL). Subsequent workup and purification steps were the same as for **4b**. Diffraction-quality green crystals of **4f** were obtained upon recrystallization. Yield: 0.143 g, 70%. R_f = 0.63 (2/1 CH_2Cl_2/hexanes). ^{1}H NMR (δ, ppm in CD_2Cl_2): 7.53−7.48 (overlapping m, 10H, aromatic C−*H*), 7.23−7.21 (m, 4H, aromatic C−*H*), 7.16−7.13 (m, 6H, aromatic C−*H*). ^{13}C NMR (δ, ppm in CD_2Cl_2): 142.0, 139.2, 130.8, 130.2, 128.0, 126.9, 126.7. IR (CH_2Cl_2, cm^{-1}): 2182 (vs, CN_{sym}), 2162 (vs, CN_{asym}). UV−vis absorption spectrum [CH_2Cl_2, λ_{max}, nm (ε_M, M^{-1} cm^{-1})]: 466 (1400), 639 (480). MALDI MS: calcd for $C_{28}H_{20}N_2S_2Ni$ *m*/*z* 507.306, obsd *m*/*z* 507.003. Cyclic voltammetry: **4f** − e^- → $[\mathbf{4f}]^+$, +0.62 V. Anal. Calcd for $C_{28}H_{20}N_2S_2Ni$: C, 69.29; H, 3.97; N, 5.52. Found: C, 66.26; H, 3.87; N, 5.56.

[($Ph_2C_2S_2$)Pd($CNMe$)$_2$] (5a). The same procedures and scale used in the synthesis of **4b** were employed but with **2** and 0.020 mL (0.38 mmol) of methyl isocyanide. Ultimately, reddish-orange diffraction-quality crystals of **5a** were obtained. Yield: 0.050 g, 78%. R_f = 0.11 (2/1 CH_2Cl_2/hexanes). ^{1}H NMR (δ, ppm in CD_2Cl_2): 7.16−7.08 (overlapping m, 10H, aromatic C−*H*), 3.45 (s, 6H, CNC*H*$_3$). ^{13}C NMR (δ, ppm in CD_2Cl_2): 145.7, 137.3, 132.7, 130.8, 129.2, 33.4 (isocyanide −*CH*$_3$). IR (CH_2Cl_2, cm^{-1}): 2246 (vs, CN_{sym}), 2230 (vs, CN_{asym}). UV−vis absorption spectrum [CH_2Cl_2, λ_{max}, nm (ε_M, M^{-1} cm^{-1})]: 421 (690), 502 (530). Cyclic voltammetry: **5a** − e^- → $[\mathbf{5a}]^+$, +0.61 V. Anal. Calcd for $C_{18}H_{16}N_2S_2Pd$: C, 50.17; H, 3.75; N, 6.50. Found: C, 49.12; H, 3.86; N, 6.48.

[($Ph_2C_2S_2$)Pd($CNBn$)$_2$] (5b). The same procedures and scale used in the synthesis and purification of **4b** were employed with **2** and 0.040 mL (0.33 mmol) of benzyl isocyanide. Diffraction-quality red crystals of **5b** were obtained. Yield: 0.057 g, 60%. R_f = 0.35 (2/1 CH_2Cl_2/hexanes). ^{1}H NMR (δ, ppm in CD_2Cl_2): 7.45−7.36 (overlapping m, 10H, Bn aromatic C−*H*), 7.17−7.07 (overlapping m, 10H, aromatic C−*H*), 4.92 (s, 4H, −CH_2−). ^{13}C NMR (δ, ppm in CD_2Cl_2): 143.1, 135.1, 131.3, 130.3, 129.7, 129.4, 127.9, 127.3, 126.4, 48.5 (−*CH*$_2C_6H_5$). IR (CH_2Cl_2, cm^{-1}): 2227 (vs, CN_{sym}), 2213 (vs, CN_{asym}). UV−vis absorption spectrum [CH_2Cl_2, λ_{max}, nm (ε_M, M^{-1} cm^{-1})]: 427 (150), 518 (50). MALDI MS: calcd for $C_{30}H_{24}N_2S_2Pd$ *m*/*z* 583.086, obsd *m*/*z* 582.733. Cyclic voltammetry: **5b** − e^- → $[\mathbf{5b}]^+$, +0.56 V. Anal. Calcd for $C_{30}H_{24}N_2S_2Pd$: C, 61.80; H, 4.15; N, 4.80; S, 11.00. Found: C, 61.20; H, 4.06; N, 4.75; S, 10.62.

[($Ph_2C_2S_2$)Pd($CNCy$)$_2$] (5c). A 0.040 mL portion (0.32 mmol) of cyclohexyl isocyanide was added to a solution of **2** (0.087 g, 0.147 mmol) in CH_2Cl_2 (25 mL). The remaining synthesis and purification steps were analogous to those used for **4b**; ultimately, red crystals of **5c** were produced. Yield: 0.067 g, 73%. R_f = 0.51 (2/1 CH_2Cl_2/hexanes). ^{1}H NMR (δ, ppm in CD_2Cl_2): 7.17−7.07 (overlapping m, 10H, aromatic C−H), 3.96 (br m, 2H, Cy), 1.93 (m, ∼4H, Cy) 1.85−1.78 (overlapping m, ∼8H, Cy), 1.45−1.50 (m, ∼8H, Cy). ^{13}C NMR (δ, ppm in CD_2Cl_2): 143.3, 135.0, 130.3, 127.8, 126.3, 55.3, 32.3, 25.2, 22.9. IR (CH_2Cl_2, cm^{-1}): 2217 (vs, CN_{sym}), 2203 (vs, CN_{asym}). UV−vis absorption spectrum [CH_2Cl_2, λ_{max}, nm (ε_M, M^{-1} cm^{-1})]: 431 (430), 504 (490). Cyclic voltammetry: **5c** − e^- → $[\mathbf{5c}]^+$, +0.61 V. Anal. Calcd for $C_{28}H_{32}N_2S_2Pd$: C, 59.30; H, 5.69; N, 4.94. Found: C, 59.47; H, 5.99; N, 4.88.

[($Ph_2C_2S_2$)Pd(CN-1-Ad)$_2$] (5e). The same procedures and scale used in the synthesis of **4b** were employed with **2** and 0.055 g (0.34 mmol) of 1-adamantyl isocyanide. Diffraction-quality, red crystals of **5e** were obtained. Yield: 0.062 g, 55%. R_f = 0.61 (2/1 CH_2Cl_2/hexanes). ^{1}H NMR (δ, ppm in CD_2Cl_2): 7.17−7.07 (overlapping m, 10H, aromatic C−*H*), 2.13 (overlapping m, 18H, Ad), 1.71 (overlapping m, 12H, Ad). ^{13}C NMR (δ, ppm in CD_2Cl_2): 143.4, 135.0, 130.3, 127.8, 126.3, 58.7, 43.2, 36.0, 29.3. IR (CH_2Cl_2, cm^{-1}): 2211 (vs, CN_{sym}), 2198 (vs, CN_{asym}). UV−vis absorption spectrum [CH_2Cl_2, λ_{max}, nm (ε_M, M^{-1} cm^{-1})]: 430 (320), 505 (420). Cyclic voltammetry: **5e** − e^- → $[\mathbf{5e}]^+$, +0.59 V. Anal. Calcd for

https://dx.doi.org/10.1021/acs.organomet.0c00375
Organometallics 2020, 39, 2854−2870

$C_{36}H_{40}N_2S_2Pd$: C, 64.41; H, 6.01; N, 4.17. Found: C, 61.86; H, 6.08; N, 3.69.

[(Ph$_2$C$_2$S$_2$)Pd(CNPh)$_2$] (5f). Phenyl isocyanide (0.040 mL, 0.38 mmol) was added to a solution of **2** (0.120 g, 0.203 mmol) in CH_2Cl_2 (25 mL). The remaining synthesis and purification steps were analogous to those implemented for compound **4b**, yielding red crystals of **5f**. Yield: 0.070 g, 66%. R_f = 0.59 (2/1 CH_2Cl_2/hexanes). ^{1}H NMR (δ, ppm in CD_2Cl_2): 7.58−7.48 (overlapping m, 10H, aromatic C−*H*), 7.21−7.19 (m, 4H, aromatic C−*H*), 7.14−7.11 (m, 6H, aromatic C−*H*). IR (CH_2Cl_2, cm^{-1}): 2198 (vs, CN_{sym}), 2182 (vs, CN_{asym}). UV−vis absorption spectrum [CH_2Cl_2, λ_{max}, nm (ε_M, M^{-1} cm^{-1})]: ∼385 (5180), ∼534 (770). Cyclic voltammetry: **5f** − e$^-$ → [**5f**]$^+$, +0.67 V.

[(Ph$_2$C$_2$S$_2$)Pt(CNMe)$_2$] (6a). The same procedures and scale used in the synthesis and purification of **4b** were employed but with **3** and methyl isocyanide (0.020 mL, 0.38 mmol). Ultimately, yellow crystals were obtained upon recrystallization by diffusion of Et_2O into a concentrated CH_2Cl_2 solution of **6a**. Yield: 0.032 g, 42%. R_f = 0.14 (2/1 CH_2Cl_2/hexanes). ^{1}H NMR (δ, ppm in CD_2Cl_2): 7.19−7.09 (unresolved m, 10H, aromatic C−*H*), 3.42 (s, 6H, CNC*H*$_3$). ^{13}C NMR (δ, ppm in CD_2Cl_2): 142.9, 135.2, 130.4, 127.9, 126.4, 30.5 (isonitrile −*C*H$_3$). IR (CH_2Cl_2, cm^{-1}): 2248 (vs, CN_{sym}), 2223 (vs, CN_{asym}). UV−vis absorption spectrum [CH_2Cl_2, λ_{max}, nm (ε_M, M^{-1} cm^{-1})]: 337 (4780). MALDI MS: calcd for $C_{18}H_{16}N_2S_2Pt$ *m*/*z* 519.554, obsd *m*/*z* 519.858. Cyclic voltammetry: **6a** − e$^-$ → [**6a**]$^+$, +0.64 V. Anal. Calcd for $C_{18}H_{16}N_2S_2Pt$: C, 41.61; H, 3.11; N, 5.39. Found: C, 41.54; H, 2.92; N, 5.44.

[(Ph$_2$C$_2$S$_2$)Pt(CNBn)$_2$] (6b). A 0.070 mL portion (0.58 mmol) of benzyl isocyanide was added to a solution of **3** (0.200 g, 0.294 mmol) in CH_2Cl_2 (20 mL). The rest of the synthesis and purification procedures were analogous to those used for compound **4b**, yielding yellow crystals of **6b**. Yield: 0.073 g, 38%. R_f 0.35 (2/1 CH_2Cl_2/hexanes). ^{1}H NMR (δ, ppm in CD_2Cl_2): 7.50−7.40 (overlapping m, 10H, aromatic C−*H*), 7.23−7.12 (overlapping m, 10H, aromatic C−*H*), 4.98 (s, 4H, −*C*H$_2$C$_6$H$_5$). ^{13}C NMR (δ, ppm in CD_2Cl_2): 142.9, 135.4, 131.5, 130.5, 129.7, 129.4, 127.9, 127.3, 126.5, 48.8 (−*C*H$_2$C$_6$H$_5$). IR (CH_2Cl_2, cm^{-1}): 2229 (vs, CN_{sym}), 2204 (vs, CN_{asym}). UV−vis absorption spectrum [CH_2Cl_2, λ_{max}, nm (ε_M, M^{-1} cm^{-1})]: 342 (1560). Cyclic voltammetry: **6b** − e$^-$ → [**6b**]$^+$, +0.57 V. Anal. Calcd for $C_{30}H_{24}N_2S_2Pt$: C, 53.64; H, 3.61; N, 4.17; S, 9.54. Found: C, 53.49; H, 3.53; N, 4.13; S, 9.36.

[(Ph$_2$C$_2$S$_2$)Pt(CNCy)$_2$] (6c). Cyclohexyl isocyanide (0.070 mL, 0.56 mmol) was added to a solution of **3** (0.203 g, 0.299 mmol) in CH_2Cl_2 (25 mL). The remaining synthesis and purification steps were analogous to those used for compound **4b**, yielding yellow crystals of **6c**. Yield: 0.084 g, 46%. R_f = 0.47 (2/1 CH_2Cl_2/hexanes). ^{1}H NMR (δ, ppm in CD_2Cl_2): 7.19−7.08 (overlapping m, 10H, aromatic C−*H*), 4.02−3.98 (m, 2H, Cy), 1.97−1.93 (m, 4H, Cy), 1.90−1.75 (overlapping m, 8H, Cy), 1.51−1.46 (m, 8H, Cy). ^{13}C NMR (δ, ppm in CD_2Cl_2): 143.1, 135.3, 130.5, 127.8, 126.3, 56.0, 32.3, 25.2, 23.0. IR (CH_2Cl_2, cm^{-1}): 2219 (vs, CN_{sym}), 2196 (vs, CN_{asym}). UV−vis absorption spectrum [CH_2Cl_2, λ_{max}, nm (ε_M, M^{-1} cm^{-1})]: 336 (9970). Cyclic voltammetry: **6c** − e$^-$ → [**6c**]$^+$, +0.67 V. Anal. Calcd for $C_{26}H_{32}N_2S_2Pt$: C, 51.27; H, 4.93; N, 4.27. Found: C, 51.19; H, 4.83; N, 4.23.

[(Ph$_2$C$_2$S$_2$)Pt(CN^{t}Bu)$_2$] (6d). The same synthesis and purification procedures used in the preparation of **4b** were employed but with 0.033 mL (0.29 mmol) of *tert*-butyl isocyanide and 0.100 g (0.147 mmol) of **3**. Ultimately, yellow crystals of **6d** were obtained upon recrystallization by diffusion of hexanes vapor into a 1,2-dichloroethane solution. Yield: 0.036 g, 41%. R_f = 0.40 (2/1 CH_2Cl_2/hexanes). ^{1}H NMR (δ, ppm in CD_2Cl_2): 7.16−7.08 (overlapping m, 10H, aromatic C−*H*), 1.58 (s, 18H, ^{t}Bu). IR (CH_2Cl_2, cm^{-1}): 2214 (vs, CN_{sym}), 2188 (vs, CN_{asym}). UV−vis absorption spectrum [CH_2Cl_2, λ_{max}, nm (ε_M, M^{-1} cm^{-1})]: 336 (10290). Cyclic voltammetry: **6d** − e$^-$ → [**6d**]$^+$, +0.66 V. Anal. Calcd for $C_{24}H_{28}N_2S_2Pt$: C, 47.75; H, 4.67; N, 4.64. Found: C, 48.09; H, 4.77; N, 4.78.

[(Ph$_2$C$_2$S$_2$)Pt(CN-1-Ad)$_2$] (6e). To a solution of **3** (0.150 g, 0.221 mmol) in CH_2Cl_2 (25 mL) was added 0.716 g (0.441 mmol) of 1-adamantyl isocyanide. Subsequent handling and purification procedures were similar to those implemented for compound **4b**, ultimately yielding yellow crystals of **6e**. Yield: 0.087 g, 52%. R_f = 0.60 (2/1 CH_2Cl_2/hexanes). ^{1}H NMR (δ, ppm in CD_2Cl_2): 7.18−7.14 (m, 4H, aromatic C−*H*), 7.12−7.08 (m, 6H, aromatic C−*H*), 2.36 (m, 18H, Ad), 1.72 (m, 12H, Ad). IR (CH_2Cl_2, cm^{-1}): 2212 (vs, CN_{sym}), 2192 (vs, CN_{asym}). UV−vis absorption spectrum [CH_2Cl_2, λ_{max}, nm (ε_M, M^{-1} cm^{-1})]: 336 (6850). MALDI MS: calcd for $C_{36}H_{40}N_2S_2Pt$, *m*/*z* 759.943, obsd *m*/*z* 760.343. Cyclic voltammetry: **6e** − e$^-$ → [**6e**]$^+$, +0.65 V. Anal. Calcd for $C_{36}H_{40}N_2S_2Pt$: C, 56.90; H, 5.31; N, 3.69. Found: C, 52.53; H, 4.71; N, 3.28.

[(Ph$_2$C$_2$S$_2$)Pt(CN^{t}Bu)$_2$][SbCl$_6$], [6d][SbCl$_6$]. The following procedure was conducted under an atmosphere of Ar in oven-dried glassware. A solution of **6d** (0.119 g, 0.198 mmol) in dry CH_2Cl_2 (10 mL) cooled to −20 °C was treated dropwise via cannula with a solution of tris(4-bromophenyl)ammoniumyl hexachloroantimonate (0.161 g, 0.197 mmol) in CH_2Cl_2 (10 mL) that was similarly chilled to −20 °C and protected from ambient light with a wrapping of Al foil. A dark green color was immediately induced in the mixture. This reaction mixture was stirred at −20 °C for 1 h in the dark, at which point the solvent was removed *in vacuo*. The residual dark solid was washed with Et_2O (3 × 5 mL) and dried under vacuum. Crystallization of [[(Ph$_2$C$_2$S$_2$)Pt(CN^{t}Bu)$_2$]$_2$][SbCl$_6$]$_2$ as irregularly shaped black crystals was accomplished by diffusion of Et_2O vapor into a CH_2Cl_2 solution held at −20 °C under N_2. This salt is unstable in air, and in solution at room temperature it readily decomposes to [(Ph$_2$C$_2$S$_2$)$_2$Pt] within minutes of exposure to air. Yield: 0.064 g, 17%. The following solution spectroscopic data are pertinent for a 2[**6d**]$^+$ ↔ [**6d**]$_2^{2+}$ equilibrium (*vide infra*), in which the former is believed to dominate: ^{1}H NMR (δ, ppm in CD_2Cl_2): 7.42−7.34 (overlapping m, 10H, aromatic C−*H*), 1.66, (s, 9H, ^{t}Bu), 1.59 (s, 9H, ^{t}Bu). IR (CH_2Cl_2, cm^{-1}): 2243 (vs, CN_{sym}), 2222 (vs, CN_{asym}). UV−vis absorption spectrum [CH_2Cl_2, λ_{max}, nm (ε_M, M^{-1} cm^{-1})]: ∼439 (910), ∼661 (1030), ∼799 (4050).

[((Ph$_2$C$_2$S$_2$)Ni(CN^{t}Bu)$_2$)$_2$(*μ*-Ag)$_2$][BF$_4$]$_2$ ([7][BF$_4$]$_2$). Under an atmosphere of Ar, a solution of $AgBF_4$ (0.029 g, 0.15 mmol) in CH_2Cl_2 (10 mL) was transferred via cannula to a solution of [(Ph$_2$C$_2$S$_2$)Ni(CN^{t}Bu)$_2$] (0.070 g, 0.15 mmol) in dry CH_2Cl_2 (10 mL). The resulting mixture was stirred overnight in the dark at 25 °C under Ar. This magenta solution was taken to dryness under reduced pressure, and the residual solid was washed with Et_2O (3 × 10 mL). Upon drying, a reddish magenta solid product was collected. Diffraction-quality crystals were obtained by slow diffusion of Et_2O vapor into a concentrated CH_2Cl_2 solution. Yield: 0.079 g, 80%. ^{1}H NMR (δ, ppm in CD_2Cl_2): 7.26−7.18 (m, 20H, aromatic C−H), 1.45 (s, 36H, ^{t}Bu). IR (CH_2Cl_2, cm^{-1}): 2211 (vs, CN_{sym}), 2198 (vs, CN_{asym}). UV−vis absorption spectrum [CH_2Cl_2, λ_{max}, nm (ε_M, M^{-1} cm^{-1})]: 523 (∼35).

[(2,6-Me$_2$py)Ni(*μ*$_2$-*η*^{1},*η*^{1}-*S*′,*η*^{1}-*S*″-S$_2$C$_2$Ph$_2$)]$_2$ (8). Via a gastight syringe, 2,6-dimethylpyridine (0.500 mL, 4.32 mmol) was delivered dropwise to a solution of **4a** (0.050 g, 0.130 mmol) in toluene (25 mL) under an argon atmosphere. The mixture was refluxed for 2 h, after which time it was cooled to room temperature. The volume of the solution was reduced by ∼2 mL under vacuum to aid in the removal of displaced MeNC ligand. Reflux in toluene was continued overnight, after which time a minimal quantity of silica gel was placed in the flask. The dark green-brown slurry was then taken to dryness *in vacuo*. The dry-loaded silica was added to the top of a column packed as a silica slurry in hexanes. Elution with 1/1 CH_2Cl_2/hexanes moved a green band of [(Ph$_2$C$_2$S$_2$)$_2$Ni] followed by brownish-orange **8**. Following collection of [(Ph$_2$C$_2$S$_2$)$_2$Ni], the latter band was fully drawn from the column using 2/1 CH_2Cl_2/hexanes. This fraction was reduced to dryness under reduced pressure, and the residual solid was washed with *n*-pentane and dried further. Recrystallization was achieved by the diffusion of hexanes vapor into a 1,2-dichloroethane solution. Yield: 0.023 g, 22%. R_f = 0.17 (2/1 CH_2Cl_2/hexanes). ^{1}H NMR (δ, ppm in CD_2Cl_2): 7.16−7.10 (m, ∼12H, aromatic C−H), 6.89−6.87 (m, ∼2H, aromatic C−H), 6.75−6.66 (m, ∼8H, aromatic C−H), 6.56−6.53 (m, ∼2H, aromatic C−H), 6.43−6.40 (m, ∼2H, aromatic C−H), 3.96 (s, 6H, −*C*H$_3$), 3.70 (s, 6H, −*C*H$_3$). UV−vis

https://dx.doi.org/10.1021/acs.organomet.0c00375
Organometallics 2020, 39, 2854−2870

absorption spectrum [CH_2Cl_2, λ_{max}, nm (ε_M, M^{-1} cm^{-1})]: 272 (8670), 364 (2800), 482 (2230), 693 (260). Cyclic voltammetry (tentative assignment): **8** − e^- → $[\mathbf{8}]^+$, +0.05 V; $[\mathbf{8}]^+$ − e^- → $[\mathbf{8}]^{2+}$, +0.67 V. Anal. Calcd for $C_{42}H_{38}N_2S_4Ni_2$: C, 61.79; H, 4.69; N, 3.43. Found: C, 61.20; H, 4.62; N, 3.45.

[($Ph_2C_2S_2$)Ni(CNMe)(PMe_3)] (9). Trimethylphosphine (0.50 mL, 5.0 mmol) was delivered dropwise via a gastight syringe to a solution of **4a** (0.039 g, 0.100 mmol) in CH_2Cl_2 (20 mL), which immediately induced formation of a purple color. The resulting mixture was stirred overnight at 25 °C, after which time the volume of solvent was reduced to ∼5 mL *in vacuo*. Addition of ∼10 mL of Et_2O led to the precipitation of a purple solid. The solvent was removed by cannula filtration, and the solid was washed with Et_2O (3 × 5 mL) to remove unreacted phosphine. The product was dried *in vacuo* for 1 h and redissolved in a minimal volume of 1,2-dichloroethane. Filtration of this concentrated solution through Celite and slow introduction of hexanes via vapor diffusion under an inert atmosphere afforded purple crystals. Yield: 0.0227 g, 53%. R_f = 0.13 (2/1 CH_2Cl_2/hexanes). ^{1}H NMR (δ, ppm in CD_2Cl_2): 7.21−7.06 (overlapping m, 10H, aromatic C−*H*), 3.44 (s, 3H, C≡NCH_3), 1.56 (d, J_{PH} = 12 Hz, 9H, −P(CH_3)$_3$). ^{13}C NMR (δ, ppm in CD_2Cl_2): 142.3, 129.70, 129.68, 127.42, 127.36, 125.7, 15.7 (d, J_{PC} = 30 Hz, P(CH_3)$_3$). ^{31}P NMR (δ, ppm in CD_2Cl_2): 3.74. IR (CH_2Cl_2, cm^{-1}): 2199 (vs, CN). UV−vis absorption spectrum [CH_2Cl_2, λ_{max}, nm (ε_M, M^{-1} cm^{-1})]: 564 (370).

[($Ph_2C_2S_2$)Ni(CNMe)(PPh_3)] (10). A solid portion of triphenylphosphine (0.113 g, 0.431 mmol) was added to a 20 mL CH_2Cl_2 solution of **4a** (0.0413 g, 0.108 mmol), which caused an immediate color change from blue to green. The resulting mixture was stirred overnight at 25 °C, after which time the solvent was removed under reduced pressure. The residual solid was purified by chromatography on a silica column packed as a slurry in hexanes. Unreacted phosphine was separated first by flash elution with 1/1 CH_2Cl_2/hexanes; continued elution with 2/1 CH_2Cl_2/hexanes moved the product as a green band. The solvent was removed under reduced pressure, and the remaining solids were washed with Et_2O. Redissolution in a minimal amount of 1,2-dichloroethane, filtration through Celite, and slow crystallization by the introduction of hexanes via vapor diffusion afforded green crystals of the product. Yield: 0.0177 g, 26%. R_f = 0.30 (2/1 CH_2Cl_2/hexanes). ^{1}H NMR (δ, ppm in CD_2Cl_2): 7.81−7.75 (m, 6H, aromatic C−*H*), 7.53−7.50 (m, 9H, aromatic C−*H*), 7.36 (m, 3H, aromatic C−*H*), 7.19−7.06 (overlapping m, 10H, aromatic C−H), 2.87 (s, 3H, C≡NCH_3). ^{31}P NMR (δ, ppm in CD_2Cl_2): 30.46. IR (CH_2Cl_2, cm^{-1}): 2204 (vs, CN). UV−vis absorption spectrum [CH_2Cl_2, λ_{max}, nm (ε_M, M^{-1} cm^{-1})]: 348 (3900), 463 (210), 622 (190). MALDI MS: calcd for $C_{34}H_{28}NPS_2Ni$ *m*/*z* 604.402, obsd *m*/*z* 604.285.

[(($Ph_2C_2S_2$)Ni(CNMe))$_2$(μ-dppb)] (11). Under an atmosphere of argon, a solution of 1,4-dppb (0.312 g, 0.699 mmol) in CH_2Cl_2 (10 mL) was added dropwise by cannulation to a solution of **4a** (0.135 g, 0.352 mmol) in CH_2Cl_2 (10 mL). The mixture was stirred at 25 °C for ∼10 h, and the progress of the reaction was attended by a change in color from blue to dark green. The solvent was then reduced in volume, and a minimal amount of silica was placed in the flask. The resulting slurry was taken to dryness *in vacuo*. The dry-loaded silica was applied directly to the top of a column packed as a slurry in hexanes. Elution with 1/1 CH_2Cl_2/hexanes moved unreacted ligand from the column; continued elution with 2/1 CH_2Cl_2/hexanes brought forward a well-resolved blue band of [($Ph_2C_2S_2$)$_2$Ni]. The desired [(($Ph_2C_2S_2$)Ni(C≡NMe))$_2$(μ-dppb)] was flushed from the column as a green band using 5% THF in CH_2Cl_2. The solvent was removed from the eluant under reduced pressure, and the solid residue was washed with ∼15 mL of pentane and dried under vacuum. The product was then dissolved in a minimal volume of CH_2Cl_2, filtered through a Celite pad, and taken to dryness again. Crystallization was accomplished by slow diffusion of Et_2O vapor into a concentrated CH_2Cl_2 solution of the product. Yield: 0.097 g, 49%. R_f = 0.81 (5% THF in CH_2Cl_2). ^{1}H NMR (δ, ppm in CD_2Cl_2): 7.85−7.79 (m, ∼6H, aromatic C−*H*), 7.74−7.69 (m, ∼4H, aromatic C−*H*), 7.56−7.47 (m, ∼10H, aromatic C−*H*), 7.19−7.06 (overlapping m, ∼24H, aromatic C−*H*), 2.71 (s, 6H, CNCH_3). ^{31}P NMR (δ, ppm in CD_2Cl_2): 30.72. IR (CH_2Cl_2, cm^{-1}): 2223 (sh), 2211 (vs, CN). UV−vis absorption spectrum [CH_2Cl_2, λ_{max}, nm (ε_M, M^{-1} cm^{-1})]: 468 (520), 618 (420). Cyclic voltammetry: **11** − 2e^- → $[\mathbf{11}]^{2+}$, + 0.51 V; $[\mathbf{11}]^{2+}$ − 2e^- → $[\mathbf{11}]^{4+}$, +1.26 V.

[(($Ph_2C_2S_2$)Pd(CNMe))$_2$(μ-dppb)] (12). The synthesis and purification procedures were analogous to those used for **11** but with 0.105 g (0.244 mmol) of **5a** and 0.217 g (0.486 mmol) of the 1,4-dppb ligand utilized. Crystallization of the product by the diffusion of Et_2O vapor into a concentrated CH_2Cl_2 solution of **12** produced violet diffraction-quality crystals. Yield: 0.121 g, 81%. R_f = 0.77 (5% THF in CH_2Cl_2). ^{1}H NMR (δ, ppm in CD_2Cl_2): 7.76−7.68 (overlapping m, ∼12H, aromatic C−*H*), 7.56−7.49 (overlapping m, ∼12H, aromatic C−*H*), 7.19−7.16 (m, ∼4H, aromatic C−H), 7.13−7.05 (m, ∼16H, aromatic C−*H*), 2.87 (s, 6H, CNCH_3). ^{31}P NMR (δ, ppm in CD_2Cl_2): 22.62. IR (CH_2Cl_2, cm^{-1}): ∼2240 (sh), 2227 (vs, CN). UV−vis absorption spectrum [CH_2Cl_2, λ_{max}, nm (ε_M, M^{-1} cm^{-1})]: ∼438 (890), ∼543 (820). Cyclic voltammetry: **12** − 2e^- → $[\mathbf{12}]^{2+}$, +0.52 V; $[\mathbf{12}]^{2+}$ − 2e^- → $[\mathbf{12}]^{4+}$, +0.93 V.

[(($Ph_2C_2S_2$)Pt(CNMe))$_2$(μ-dppb)] (13). The synthesis and purification procedures were analogous to those employed for **11** but with 0.246 g (0.473 mmol) of **6a** and 0.422 g (0.945 mmol) of the 1,4-dppb ligand utilized. Diffusion of Et_2O vapor into a concentrated CH_2Cl_2 solution of **13** produced bright yellow, diffraction-quality crystals. Yield: 0.119 g, 36%. R_f = 0.75 (5% THF in CH_2Cl_2). ^{1}H NMR (δ, ppm in CD_2Cl_2): 7.80−7.73 (overlapping m, 8H, aromatic C−*H*), 7.57−7.46 (overlapping m, 8H, aromatic C−*H*), 7.20−7.10 (overlapping m, 28H, aromatic C−*H*), 3.48 (s, 6H, CNCH_3). ^{31}P NMR (δ, ppm in CD_2Cl_2): 14.94 (s, J_{Pt-P} = 2655 Hz). IR (CH_2Cl_2, cm^{-1}): ∼2237 (sh), 2222 (vs, CN). UV−vis absorption spectrum [CH_2Cl_2, λ_{max}, nm (ε_M, M^{-1} cm^{-1})]: 340 (11800). Cyclic voltammetry: **13** − 2e^- → $[\mathbf{13}]^{2+}$, +0.57 V; $[\mathbf{13}]^{2+}$ − 2e^- → $[\mathbf{13}]^{4+}$, +1.26 V.

[Et_4N]$_2$[($Ph_2C_2S_2$)Ni($CN)_2$] ([Et_4N]$_2$[15]). The following is a better-yielding alternative to a preparation reported earlier.[10] A solution of [Et_4N]$_2$[Ni($CN)_4$] (0.035 g, 0.083 mmol) in 10 mL of MeCN (10 mL) was added to a solution of **4a** (0.030 g, 0.078 mmol) in 10 mL of MeCN, which produced a change in color from dark blue to maroon. The solution was stirred overnight under an inert atmosphere, after which time the solution volume was reduced to ∼3 mL. Addition of 10 mL of Et_2O induced precipitation of a red solid. The Et_2O was decanted by use of a cannula, and the solid was dried *in vacuo* for 1 h. Redissolution in a minimal volume of MeCN, filtration through Celite, and slow crystallization by the introduction of Et_2O via vapor diffusion afforded red crystals of [Et_4N]$_2$[**15**]. Yield: 0.016 g, 0.026 mmol, 35%. ^{1}H NMR (δ, ppm in CD_3CN): 7.16−7.11 (m, 4H, aromatic C−H), 7.09−7.02 (m, 6H, aromatic), 3.36−3.29 (q, 16H, N(CH_2CH_3)$_4^+$), 1.30 (t, $J \approx 5$ Hz, 24H, N(CH_2CH_3)$_4^+$). ^{13}C NMR (δ, ppm in CD_3CN): 145.0, 138.0, 131.1, 130.6, 128.9, 126.8, 53.8 (−CH_2−, Et_4N^+), 8.4 (−CH_3, Et_4N^+). IR (CH_3CN, cm^{-1}): 2111 (vs, CN_{sym}), 2099 (vs, CN_{asym}). UV−vis absorption spectrum [CH_2Cl_2, λ_{max}, nm (ε_M, M^{-1} cm^{-1})]: 489 (220), 378 (5380). Cyclic voltammetry: $[\mathbf{15}]^{2-}$ − e^- → $[\mathbf{15}]^-$, −0.07 V.

[Et_4N][($Ph_2C_2S_2$)Pd(CN)(CNMe)] ([Et_4N][16]). Under an atmosphere of Ar, [Et_4N][CN] (0.100 g, 0.64 mmol) was added to a solution of **5a** (0.138 g, 0.32 mmol) in CH_3NO_2 (25 mL) and the mixture was refluxed overnight with stirring. A gradual color change from red to dark orange was observed as the reaction progressed. After being cooled, the solution was then reduced in volume, and a minimal amount of neutral alumina (∼1.0 g) was placed in the flask. The resulting slurry was taken to dryness *in vacuo*. The dry-loaded alumina was applied directly to the top of a neutral alumina column packed as a slurry in 1/1 CH_2Cl_2/CH_3CN. The column was then eluted with this same solvent mixture. A red band of unreacted **5a** was collected followed by a well-resolved dark orange band of [Et_4N][**16**], which was fully flushed from the column with 100% CH_3CN. The solvent was removed from the eluant *in vacuo*, and the residue was washed with Et_2O (3 × 10 mL). The residual solid was then dissolved in a minimal volume of CH_3CN, and the resulting solution was filtered through a Celite pad and taken to dryness again. Crystallization of [Et_4N][**16**] was accomplished by slow diffusion of

https://dx.doi.org/10.1021/acs.organomet.0c00375
Organometallics 2020, 39, 2854−2870

Scheme 3. Synthesis of Group 10 Dithiolene Bis(isonitrile) Compounds

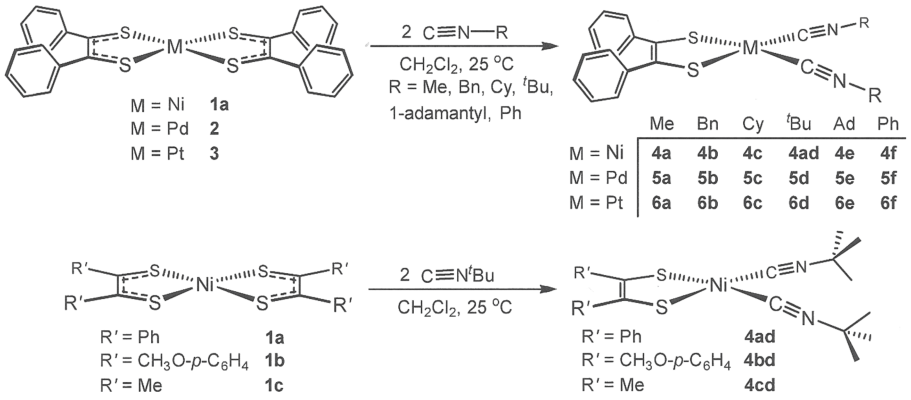

Et_2O vapor into a concentrated CH_3CN solution. Yield: 0.104 g, 59%. R_f = 0.69 (1/1 CH_2Cl_2/CH_3CN). ^1H NMR (δ, ppm in CD_3CN): 7.11−7.01 (m, 10H, aromatic C−*H*), 3.41 (s, 3H, $CNCH_3$), 3.16 (q, 8H, $N(CH_2CH_3)_4^+$), 1.19 (t, 12H, $N(CH_2CH_3)_4^+$). IR (CH_2Cl_2, cm^{-1}): 2227 (vs, C≡NMe), 2120 (s, −C≡N). UV−vis absorption spectrum [CH_2Cl_2, λ_{max}, nm (ε_M, M^{-1} cm^{-1})]: 338 (9800), 535 (920). Cyclic voltammetry: $[\mathbf{16}]^- - e^- \rightarrow [\mathbf{16}]$, +0.27 V.

[Et_4N][($Ph_2C_2S_2$)Pt(CN)(CNMe)] ([Et_4N][17]). The same synthesis and purification procedures used in the synthesis of [Et_4N][**16**] were employed but with 0.060 g (0.38 mmol) of [Et_4N][CN] and 0.066 g (0.13 mmol) of **6a**. Diffraction-quality crystals were obtained by slow diffusion of Et_2O vapor into a saturated CH_3CN solution of the reddish orange product. Yield: 0.040 g, 49%. R_f = 0.74 (1/1 CH_2Cl_2/CH_3CN). ^1H NMR (δ, ppm in CD_2Cl_2): 7.17−7.11 (m, 4H, aromatic C−*H*), 7.10−7.03 (m, 6H, aromatic C−*H*), 3.38 (s, 3H, $CNCH_3$), 3.24 (q, 8H, $N(CH_2CH_3)_4^+$), 1.26 (t, 12H, $N(CH_2CH_3)_4^+$). ^{13}C NMR (δ, ppm in CD_2Cl_2): 144.4 (C≡NR, C≡N), 135.5, 130.4, 127.6, 125.8, 125.7, 53.2 ($N(CH_2CH_3)_4^+$), 30.2 ($CNCH_3$), 7.9 ($N(CH_2CH_3)_4^+$). IR (CH_2Cl_2, cm^{-1}): 2219 (vs, C≡NMe), 2120 (s, $^-$C≡N). UV−vis absorption spectrum [CH_2Cl_2, λ_{max}, nm (ε_M, M^{-1} cm^{-1})]: 497 (1350). Cyclic voltammetry: $[\mathbf{17}]^- - e^- \rightarrow [\mathbf{17}]$, +0.26 V.

[($Ph_2C_2S_2$)Ni(IPr)(CNMe)] (18). The synthesis, purification, and characterization of **18** have been described previously.[10]

[($Ph_2C_2S_2$)Pd(IPr)(CNMe)] (19). The synthesis and purification procedures were analogous to those used for **18** but with 0.050 g (0.116 mmol) of **5a** and 0.090 g (0.232 mmol) of IPr.[10] Purification was accomplished by flash column chromatography from a silica column eluted with 2/1 CH_2Cl_2/hexanes followed by 100% CH_2Cl_2 to collect **19** as an orange fraction. Crystallization of **19** as orange needle crystals was accomplished by the diffusion of hexanes vapor into a concentrated 1,2-dichloroethane solution. Yield: 0.0465 g, 51%. R_f = 0.70 (5% THF in CH_2Cl_2). ^1H NMR (δ, ppm in CD_2Cl_2): 7.58 (t, J = 6 Hz, 2H, aromatic C−*H*), 7.40 (d, J = 6 Hz, 4H, aromatic C−*H*), 7.25 (s, 2H, carbene −C*H*=*H*C−), 7.06−6.97 (overlapping m, 10H, aromatic C−*H*), 3.24 (s, 3H, $CNCH_3$), 2.96 (septet, J = 6 Hz, 4H, IPr −C*H*(CH_3)$_2$), 1.40 (d, J = 6 Hz, 12H, IPr −CH(CH_3)$_2$), 1.16 (d, J = 6 Hz, 12H, IPr −CH(CH_3)$_2$). ^{13}C NMR (δ, ppm in CD_2Cl_2): 177.7, 146.3, 144.4, 135.9, 130.7, 130.5, 130.3, 127.4, 127.3, 125.6, 125.4, 124.6, 29.3 ($CNCH_3$), 26.5 (IPr, −CH(CH_3)$_2$), 22.9 (IPr, −CH(CH_3)$_2$). IR (CH_2Cl_2, cm^{-1}): 2213 (vs, CN). UV−vis absorption spectrum [CH_2Cl_2, λ_{max}, nm (ε_M, M^{-1} cm^{-1})]: 470 (370). Cyclic voltammetry: $\mathbf{19} - e^- \rightarrow [\mathbf{19}]^+$, +0.33 V.

[($Ph_2C_2S_2$)Pt(C(NMe)(IPr))(CNMe)] (20). The scale of the synthesis and procedure for purification were the same as those detailed for **19**. Crude **20** was purified by flash column chromatography from a silica column eluted with 2/1 CH_2Cl_2/hexanes followed by 5% THF in CH_2Cl_2 to flush it from the column as a dark yellow band. After removal of the eluting solvents, crystallization of **20** was accomplished by the diffusion of hexanes vapor into a concentrated 1,2-dichloroethane solution. Yield: 0.0166 g, 19%. R_f = 0.75 (5% THF in CH_2Cl_2). ^1H NMR (δ, ppm in CD_2Cl_2): 7.56 (t, $J \approx 8$ Hz, 2H, aromatic C−H), 7.32 (d, $J \approx 8$ Hz, 4H, aromatic C−H) 7.14 (s, 2H, carbene −C*H*=*H*C−), 7.12−6.99 (overlapping m, 10H, aromatic C−*H*), 3.24 (s, 3H, −CH_3), 3.03 (s, 3H, − CH_3), 2.90 (septet, $J \approx 6$ Hz, 4H, IPr −C*H*(CH_3)$_2$), 1.26 (d, J = 6 Hz, 12H, IPr −CH(CH_3)$_2$), 1.14 (d, J = 6 Hz, 12H, IPr −CH(CH_3)$_2$). IR (CH_2Cl_2, cm^{-1}): 2213 (vs, CN). UV−vis absorption spectrum [CH_2Cl_2, λ_{max}, nm (ε_M, M^{-1} cm^{-1})]: 344 (7530). Cyclic voltammetry: $\mathbf{20} - e^- \rightarrow [\mathbf{20}]^+$, +0.28 V.

[($Ph_2C_2S_2$)Ni(CNMe)(C(NHMe)(NMe_2))] (21). Under an Ar atmosphere, tetraisopropylbenzobisimidazolium dibromide (0.100 g, 0.20 mmol) was transferred into an oven-dried 100 mL Schlenk flask followed by NaH (0.020 g, 0.82 mmol) and a catalytic amount of potassium *tert*-butoxide introduced via the tip of a spatula. The flask was affixed to a Schlenk line, and the mixture of solids was suspended in dry THF (50 mL). The mixture was stirred at 25 °C for ∼14 h, during which time smooth bubbling of H_2 gas was observed. Separation of the deprotected carbene ligand from the insoluble materials in the mixture was achieved by filtration through a Schlenk frit padded with 1 in. of Celite. The filtrate was transferred dropwise via cannula into a Schlenk flask containing a solution of **4a** (0.08 g, 0.2 mmol) in dry THF (10 mL). The resulting mixture was stirred for 8 h at 25 °C, during which time the color changed from dark blue to magenta and then to red. The solvent was removed *in vacuo*, and the red residual solid was washed with Et_2O (3 × 10 mL). After being dried under vacuum, **21** was crystallized in diffraction-quality form by slow diffusion of CH_3O^tBu vapor into a concentrated 1,2-dichloroethane solution. Yield: 0.081 g, 91%. ^1H NMR (δ, ppm in CD_2Cl_2): 7.19−7.01 (overlapping m, 10H, aromatic C−*H*), 5.55 (br, 1H, −N*H*CH_3 carbene), 3.92 (s, 3H, −CH_3), 3.71 (d, J = 6 Hz, 3H, −NHC*H*$_3$ carbene), 3.35 (s, 3H, −CH_3), 2.94 (s, 3H, −CH_3). ^{13}C NMR (δ, ppm in CD_2Cl_2): 204.9, 143.6, 143.3, 137.9, 136.8, 130.2, 130.0, 127.7, 127.6, 125.6, 47.6, 36.6, 36.5, 30.3. IR (CH_2Cl_2, cm^{-1}): 2197 (vs, CN). UV−vis absorption spectrum [CH_2Cl_2, λ_{max}, nm (ε_M, M^{-1} cm^{-1})]: 510 (200). Cyclic voltammetry: $\mathbf{24} - e^- \rightarrow [\mathbf{24}]^+$, +0.35 V.

RESULTS AND DISCUSSION

Synthesis and Structures. The formation of [($Ph_2C_2S_2$)-M(C≡NR)$_2$] from [($Ph_2C_2S_2$)$_2$M] occurs readily under ambient conditions upon the introduction of 2 equiv of C≡NR (Scheme 3, top). With a constant metal (Ni^{2+}) and isocyanide ligand (CN^tBu), variation in the dithiolene ligand substituent among the set R′ = Me, Ph, *p*-anisyl has no important effect upon either yield or physical properties (Scheme 3, bottom). These products are generally amenable to column chromatographic purification and standard methods of crystallization.

In our preceding report,[10] several members of the set **4a−f**, **5a−f**, and **6a−f** were described structurally (**4a**, **5d**, **6f**). In this succeeding work, the structures of the remaining members and

https://dx.doi.org/10.1021/acs.organomet.0c00375
Organometallics 2020, 39, 2854−2870

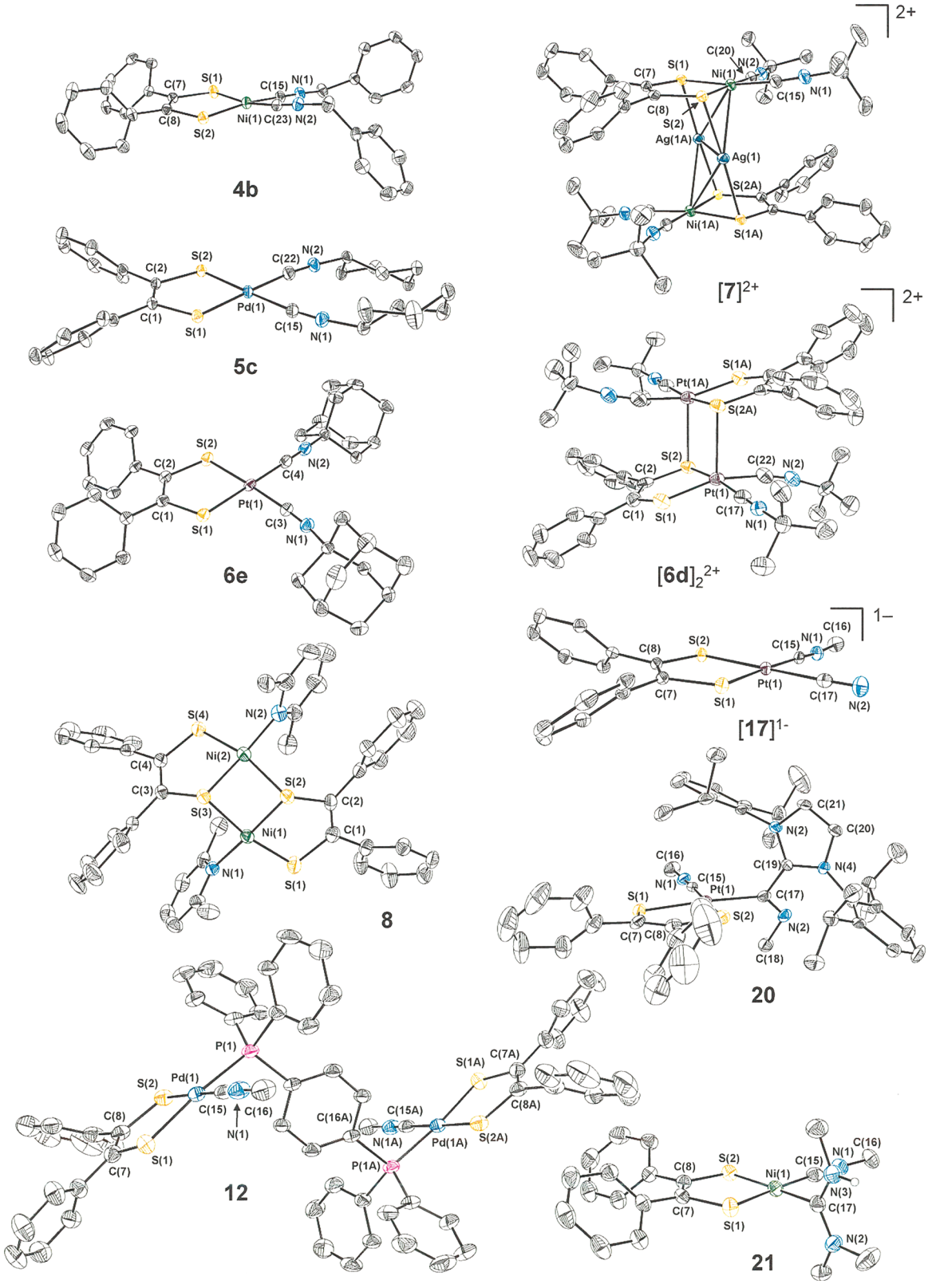

Figure 1. Representative thermal ellipsoid plots at the 50% probability level of compounds from Schemes 3−5. Hydrogen atoms are omitted for clarity.

of a variant with a different dithiolene ligand (**4bd**) are joined to the array of crystallographic data. Unit cell, refinement indices and other pertinent crystallographic data are available in Tables S1−S4 in the Supporting Information, while representative structures are depicted in Figure 1. Selected bond lengths and angles, presented where possible as averaged values, are gathered in Table 1. Considered in the aggregate, these data identify several trends: 1) A tendency toward

https://dx.doi.org/10.1021/acs.organomet.0c00375
Organometallics 2020, 39, 2854−2870

Table 1. Selected Bond Lengths (Å) and Angles (deg) for 4a−f, 5a−f, and 6a−f[a]

	4a	4b	4c[g]	4d[h]	4e	4f
Ni−C_{ave}[b]	1.8551[9][f]	1.8454[13]	1.848[2]	1.8498(17)	1.848[2]	1.8507[13]
Ni−S_{ave}	2.1427[3]	2.1404[4]	2.1402[2]	2.1344(5)	2.1346[5]	2.1485[6]
Δ[c]	0.288	0.295	0.292	0.285	0.287	0.298
S−C_{ave}	1.7649[8]	1.7571[12]	1.761[2]	1.7577(16)	1.760[2]	1.7688[12]
C−$C_{chelate}$	1.348[1]	1.354(2)	1.346[3]	1.343(3)	1.351[3]	1.355(2)
C≡N_{ave}	**1.149[1]**	**1.152[1]**	**1.149[2]**	**1.149(2)**	**1.147[2]**	**1.162[1]**
C−Ni−C	89.91[5]	93.44(7)	90.68[11]	93.83(10)	89.15[10]	96.15(8)
S−Ni−S	90.478[13]	90.613(18)	91.10[3]	90.32(2)	90.79[3]	90.35(3)
S−Ni−$C_{cis,ave}$	90.18[3]	88.68[4]	89.87[5]	89.02(5)	90.60[5]	88.41[4]
S−Ni−$C_{trans,ave}$	173.44[3]	170.71[4]	169.13[5]	168.83(5)	171.51[5]	165.84[4]
θ[d] (deg)	6.5, 12.2	12.6	14.7, 19.9,12.5	15.6	11.7, 13.4	19.2
δ[e] (Å)	0.064, 0.121	0.127	0.147, 0.194, 0.121	0.155	0.113, 0.132	0.195
	5a	**5b**	**5c**	**5d**	**5e**	**5f**
Pd−C_{ave}[b]	2.002[1][f]	1.994[2]	1.9982[11]	1.9955(13)	1.9945[2]	2.0010[13]
Pd−S_{ave}	2.2684[1]	2.2708[4]	2.2650[3]	2.2604(3)	2.2625[5]	2.2641[4]
Δ[c]	0.266	0.277	0.267	0.265	0.268	0.263
S−C_{ave}	1.762[1]	1.761[1]	1.7652[9]	1.7606(12)	1.765[2]	1.7668[11]
C−$C_{chelate}$	1.351(3)	1.352(3)	1.3555(17)	1.351(2)	1.347(3)	1.356(2)
C≡N_{ave}	**1.135[2]**	**1.145[2]**	**1.1442[14]**	**1.1465(17)**	**1.145[3]**	**1.146[1]**
C−Pd−C	91.8[4][i]	92.07(1)	88.48(6)	93.33(7)	96.79(10)	92.20(7)
S−Pd−S	88.87(2)	88.940(19)	88.678(12)	88.028(16)	88.76(2)	88.356(15)
S−Pd−$C_{cis,ave}$	89.6[3][i]	89.63[5]	91.44[3]	89.92(4)	87.27[5]	90.76[4]
S−Pd−$C_{trans,ave}$	175.7[2][i]	175.52[5]	178.64[3]	171.28(4)	175.27[5]	175.13[4]
θ[d] (deg)	2.3, 8.7[j]	5.5	1.9	11.7	3.3	4.4
δ[e] (Å)	0.083, 0.024	0.059	0.020	0.123	0.036	0.044
	6a	**6b**	**6c**	**6d**	**6e**	**6f**
Pt−C_{ave}[b]	1.955[2][f]	1.973[2]	1.964[3]	1.965[2]	1.957[2]	1.965[3]
Pt−S_{ave}	2.2757[5]	2.2829[6]	2.2747[7]	2.2773[5]	2.2745[6]	2.2748[7]
Δ[c]	0.321	0.310	0.311	0.312	0.318	0.310
S−C_{ave}	1.765[2]	1.760[2]	1.762[2]	1.763[2]	1.760[2]	1.764[3]
C−$C_{chelate}$	1.349[4]	1.353(4)	1.353(3)	1.343(4)	1.353(4)	1.345(5)
C≡N_{ave}	**1.146[3]**	**1.134[3]**	**1.136[3]**	**1.145[3]**	**1.150[3]**	**1.138[4]**
C−Pt−C	91.38[11]	91.43(12)	88.36(16)	96.13(12)	96.08(13)	90.70(7)
S−Pt−S	88.74[2]	89.13(3)	88.77(3)	89.12(2)	88.84(3)	91.512(17)
S−Pt−$C_{cis,ave}$	89.97[6]	89.78[6]	91.45[8]	87.37[6]	87.58[7]	89.99[4]
S−Pt−$C_{trans,ave}$	177.67[6]	178.51[6]	178.50[6]	176.27[6]	175.66[7]	176.67[4]
θ[d] (deg)	3.7, 1.6	4.1	2.1	1.9	3.2	4.0
δ[e] (Å)	0.039, 0.013	0.044	0.021	0.008	0.034	0.041

[a]The structures of **4a**, **5d**, and **6f** were reported previously.[7] Structural data are included here to assist identification of general trends. [b]Uncertainties are propagated according to Taylor, J. R. *An Introduction to Error Analysis*, 2nd ed.; University Science Books: Sausalito, CA. 1997; pp 73−77. [c]Δ = M−S_{ave} − M−C_{ave}. [d]θ = angle between C−M−C and S−M−S planes. [e]Average atom displacement from MS_2C_2 mean plane. [f]Brackets designate propagated uncertainty. [g]Values are from one whole molecule and two half molecules on special positions in the unit cell. [h]Values are not averaged, as only a half molecule occurs in the asymmetric unit of the cell. [i]High uncertainties originate from the presence of a disordered MeNC, which was used in averaging. [j]Two values occur due to a MeNC ligand disordered over two positions.

greater planarity, as gauged by θ, the angle between the MS_2 and MC_2 planes, and by δ, the average atom displacement (Å) from the MS_2C_2 mean plane, upon descending the group 10 metals from Ni to Pd to Pt (Table 1). This progression is due to the stronger ligand field enjoyed by the second- and third-row metals, in a constant ligand environment, in comparison to a first-row metal. 2) A lower value of Δ, the difference between M−S and M−C bond lengths, in moving from Ni to Pd and then an increase in moving from Pd to Pt. This change arises from either an enhanced Pd−S interaction or diminished Pd−C bonding—or both—relative to the Ni and Pt compounds. 3) A modest decrease in the isonitrile C≡N bond length in moving from Ni^{2+} to Pd^{2+} to Pt^{2+} at parity of ligand such that, in more instances than not, the difference in C≡N for the nickel compound vs the platinum compound is significant by the 3σ criterion (Table 1, boldface type). The meaningfulness of this trend is corroborated by ν_{CN} (*vide infra*), which moves to higher energy as the metal varies from Ni^{2+} to Pd^{2+} to Pt^{2+}.

Compounds of the type $[(Ph_2C_2S_2)M(C{\equiv}NR)_2]$ generally support a single one-electron oxidation at ∼+0.50 V vs AgCl/Ag (*vide infra*), which is attributed to the transformation of the ene-1,2-dithiolate to a radical monoanion (Scheme 1). Among redox agents with oxidizing power nominally sufficient to generate cationic $[(Ph_2C_2S_2)M(C{\equiv}NR)_2]^+$ is Ag^+ in CH_2Cl_2.[19] Introduction of $AgBF_4$ in CH_2Cl_2 to $[(Ph_2C_2S_2)$-$Ni(C{\equiv}N^tBu)_2]$ produces dimetallic $[[(Ph_2C_2S_2)Ni(C{\equiv}N^tBu)_2]_2(\mu\text{-}Ag)_2][BF_4]_2$ ([**7**][BF_4]$_2$; Scheme 4), wherein two closely juxtaposed Ag^+ ions are flanked by the dithiolene sulfur atoms of two parallel $[(Ph_2C_2S_2)Ni(C{\equiv}N^tBu)_2]$ units such that the midpoint of the Ag_2^{2+} unit coincides with an inversion

https://dx.doi.org/10.1021/acs.organomet.0c00375
Organometallics 2020, 39, 2854−2870

Scheme 4. Outcomes from the Reaction of $[(Ph_2C_2S_2)M(CN^tBu)_2]$ with Oxidizing Agents

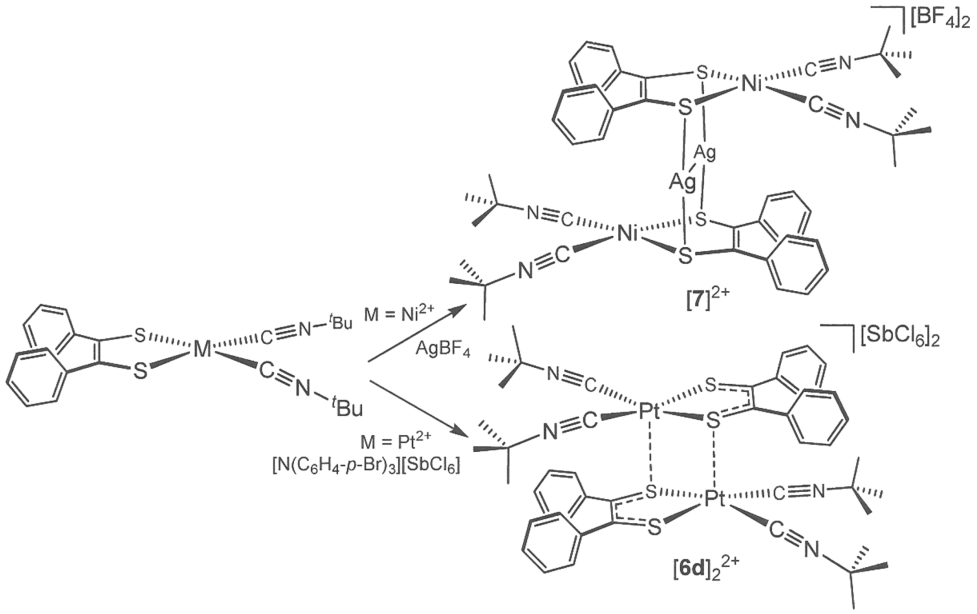

center and only half of the overall assembly is structurally unique. Intraligand S−C and C−$C_{chelate}$ bonds in $[7]^{2+}$ (Table 2 and Scheme 1) remain consistent with the ene-1,2-dithiolate formulation of the ligand and indicate that electron transfer did not occur. Rather, the Ag^+ ions have simply been ensconced between the soft thiolate sulfur atoms. A similar outcome was found with [(dcpe)Ni($S_2C_6H_2S_2$)Ni(dcpe)] (dcpe = 1,2-bis(dicyclohexylphosphino)ethane; $[S_2C_6H_2S_2]^{4-}$ = 1,2,4,5-tetrathiolatobenzene) in reaction with Ag[B(3,5-$(CF_3)_2$-$C_6H_3)_4$],[20] and other complexes featuring the Ag_2^{2+} unit in an environment of sulfur donor atoms have been described.[21,22]

Table 2. Selected Bond Lengths (Å) and Angles (deg) for $[7]^{2+}$ and $[\mathbf{6d}]_2^{2+}$

$[7]^{2+}$		$[\mathbf{6d}]_2^{2+}$	
Ni−C_{ave}	1.863[2]	Pt−C[d]	1.986[7]
Ni−S_{ave}	2.1631[4]	Pt−C[e]	1.997[9]
Δ[a]	0.300	Pt−S[f]	2.263[1]
S−C_{ave}	1.7626[13]	Pt−S[g]	2.272[1]
C−$C_{chelate}$	1.348(2)	Δ[a]	0.276
C≡N_{ave}	1.146[2]	C≡N_{ave}	1.131[6]
S−Ag_{ave}	2.4403[4]	Pt···S[h]	2.749[1]
Ni−Ag_{ave}	2.9442[2]	S−C[i]	1.708[7]
Ag···Ag	3.0921(3)	S−C[j]	1.726[7]
Ni···Ni	5.011	C−$C_{chelate}$	1.384[9]
δ[b] (Å)	0.054	δ[b] (Å)	0.216, 0.223
C−Ni−C	92.94(9)	C−Pt−C	90.2[3]
S−Ni−S	90.877(19)	S−Pt−S[k]	87.70[6]
S−Ni−$C_{cis,ave}$	88.26[5]	S_{br}−Pt−S_{br}[l]	94.58[5]
S−Ni−$C_{trans,ave}$	173.85[4]	$S_{non\ br}$−Pt−S_{br}[m]	103.42[6]
Ag−Ni−Ag	63.352(7)	S−Pt−$C_{trans,\ non\ br}$[n]	162.4[2]
Ni−Ag−Ni	116.648(7)	S−Pt−$C_{trans,\ br}$[o]	173.1[2]
θ[c] (deg)	8.7	θ[c] (deg)	18.3, 18.9

[a]Δ = M−S_{ave} − M−C_{ave}. [b]Displacement of M above the S_2C_2 mean plane. [c]θ = angle between C_2M and S_2M planes. [d]Isonitrile carbon *trans* to bridging sulfur. [e]Isonitrile carbon *cis* to bridging sulfur. [f]Dithiolene sulfur not involved in bridging. [g]Dithiolene sulfur involved in bridging. [h]Pt···S interaction through which dimerization occurs. [i]Dithiolene sulfur not involved in dimer formation. [j]Dithiolene sulfur involved in dimeric interaction. [k]Intraligand S−Pt−S angle; [l]Dithiolene sulfur atoms involved in bridging. [m]Angle defined by nonbridging sulfur and bridging dithiolene sulfur from the other half of the dimer. [n]*trans* S−Pt−C angle involving dithiolene sulfur not involved in bridging; [o]*trans* S−Pt−C angle involving dithiolene sulfur involved in bridging.

Triarylaminium cations such as $[N(C_6H_4\text{-}p\text{-}Br)_3]^+$ both are more potent oxidizing agents and are uncomplicated by any tendency to act as a ligand. Treatment of a CH_2Cl_2 solution of $[(Ph_2C_2S_2)Pt(C{\equiv}N^tBu)_2]$ with $[N(C_6H_4\text{-}p\text{-}Br)_3][SbCl_6]$ induces an immediate and pronounced darkening in color. Following removal of $[N(C_6H_4\text{-}p\text{-}Br)_3]$ upon washing, recrystallization from CH_2Cl_2/Et_2O provides crystalline $[[(Ph_2C_2S_2)Pt(C{\equiv}N^tBu)_2]_2][SbCl_6]_2\cdot 2CH_2Cl_2$ ($[\mathbf{6d}]_2[SbCl_6]_2\cdot 2CH_2Cl_2$), which was identified by X-ray crystallography. Dimerization occurs via long Pt···S interactions (~2.75 Å, Table 2) that are enabled by moderate pyramidalization at the Pt^{2+} ions. This pyramidalization lifts the Pt^{2+} ions ~0.22 Å above the S_2C_2 mean plane and folds the PtS_2 and PtC_2 planes to a dihedral angle of ~18.5° from their near planarity in charge-neutral **6d** (Table 2). The center of the resulting Pt_2S_2 rhomb resides on an inversion center in the triclinic space group $P\bar{1}$. Intraligand S−C and C−$C_{chelate}$ bond lengths in $[\mathbf{6d}]_2^{2+}$ are appreciably shorter and longer, respectively, than the corresponding values in **6d** (cf. Table 1). These bond length changes indicate transformation of the dithiolene ligand from an ene-1,2-dithiolate to a radical monoanion (Scheme 1), which simultaneously introduces multiple-bond character between sulfur and carbon and lowers the C−$C_{chelate}$ bond order. The general dimeric structure exemplified in $[\mathbf{6d}]_2^{2+}$ is typical for homoleptic $[M(S_2C_2R_2)_2]^{0,1-,2-}$ (M = Fe, Co) complexes[23,24] but is a less common structure type for heteroleptic transition-metal dithiolene complexes. A similar dimeric structure held by axial Pt···S interactions has been observed for $[[((^tBu\text{-}p\text{-}C_6H_4)_2C_2S_2)Pt(4,4'\text{-}^tBu_2\text{-bipy})]_2][PF_6]_2$.[25]

https://dx.doi.org/10.1021/acs.organomet.0c00375
Organometallics 2020, 39, 2854−2870

Scheme 5. Substitution Reactions of $[(Ph_2C_2S_2)M(CNCH_3)_2]$ (M = Ni^{2+}, Pd^{2+}, Pt^{2+})

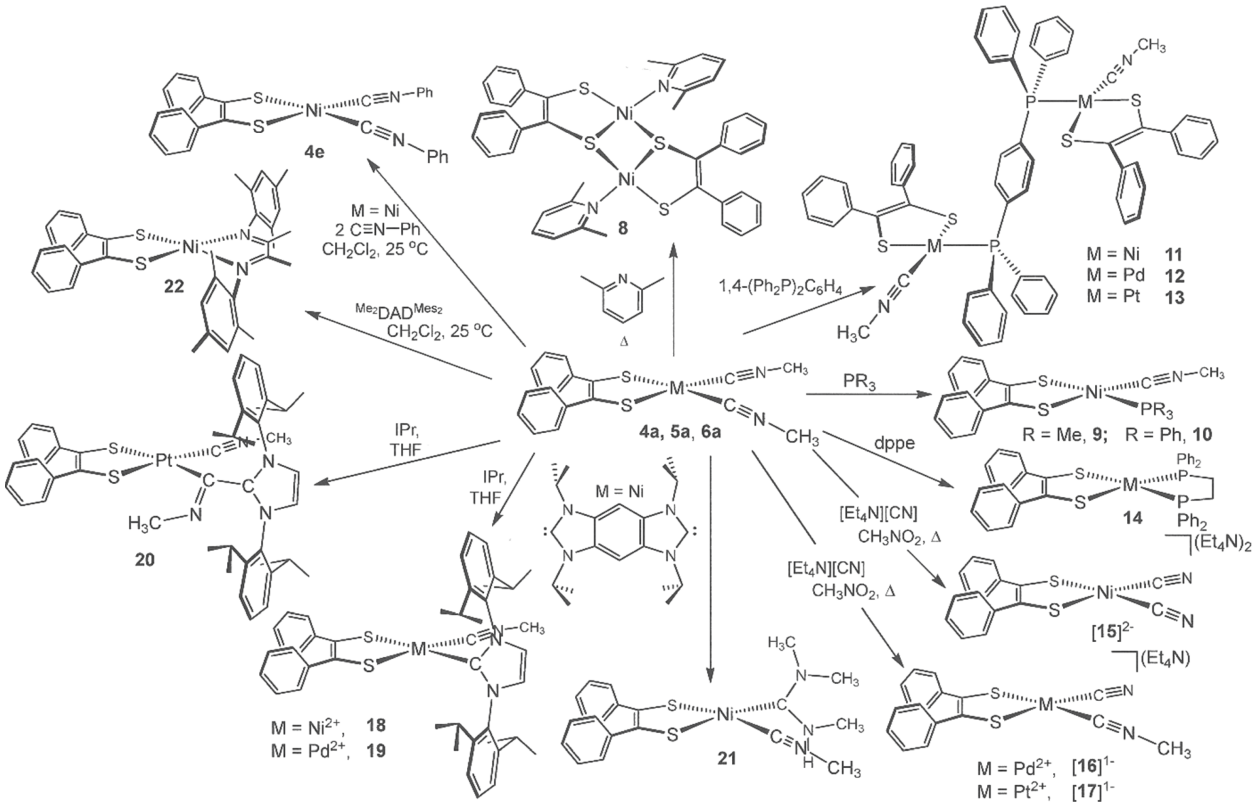

Following an initial limited set of observed displacements of MeNC from $[(Ph_2C_2S_2)Ni(C{\equiv}NMe)_2]$,[10] we have more thoroughly probed the breadth of substitution reactions that can be accomplished by new ligands across the $[(Ph_2C_2S_2)M(C{\equiv}NMe)_2]$ (M = Ni^{2+}, Pd^{2+}, Pt^{2+}) series. Scheme 5 presents the full range of results observed thus far with $[(Ph_2C_2S_2)M(C{\equiv}NMe)_2]$ (M = Ni^{2+}, Pd^{2+}, Pt^{2+}), including those disclosed previously. Treatment of **4a** with excess 2,6-dimethylpyridine led to modest yields of dimetallic **8**, which is noteworthy among the compounds of Scheme 5 in being only one of two outcomes showing complete displacement of MeNC by a monodentate ligand. The two Ni^{2+} ions are bridged by one thiolate sulfur from each dithiolene ligand but in a slightly asymmetric fashion, in which the shorter Ni–S bond is formed with the sulfur atom from the dithiolene ligand that chelates the metal ion. The difference in Ni–S_{br} bond lengths is ~0.07 Å (Table 3). The central Ni_2S_2 core shows a distinctive "butterfly" fold along the Ni···Ni axis such that the two Ni–S_{br}–Ni planes meet at a 62.8° angle (Figure 1). The nearly planar C_2S_2Ni metallodithiolene groups at the two ends of the molecule are, as a consequence of the folding within the central Ni_2S_2 core, disposed at an angle of 74.3°. Similar structural features have been observed in dipalladium dithiolene complexes bearing Ph_3P in place of 2,6-dimethylpyridine.[26,27]

With either PPh_3 or PMe_3, substitution of MeNC in $[(Ph_2C_2S_2)Ni(CNMe)_2]$ leads only to $[(Ph_2C_2S_2)Ni(CNMe)(PMe_3)]$ (**9**) and $[(Ph_2C_2S_2)Ni(CNMe)(PPh_3)_2]$ (**10**), both of which have been identified spectroscopically and structurally by X-ray diffraction. With the kinetic advantage of the chelate effect, 1,2-bis(diphenylphosphino)ethane (dppe) effects a second displacement of MeNC and produces $[(Ph_2C_2S_2)Ni(dppe)]$ (**14**). An enhanced M–CNMe interaction in **9** and **10** is clearly manifested by a Ni–CNMe bond length that is shortened by ~0.03 Å relative to that in **4a** (cf. Tables 1 and 4) and by the greater resistance of this second isocyanide ligand to a second ligand substitution. As anticipated in view of the outcome found with PPh_3, use of 1,4-bis(diphenylphosphino)-benzene with $[(Ph_2C_2S_2)M(CNMe)_2]$ yields dimetallic $[(Ph_2C_2S_2)M(CNMe)]_2(\mu\text{-}1,4\text{-}(Ph_2P)_2C_6H_4)$ (M = Ni^{2+} (**11**), Pd^{2+} (**12**), Pt^{2+} (**13**)) (Scheme 5 and Figure 1). Although crystals of **11**–**13** were grown under the same conditions, **11** crystallizes on a general position in triclinic space group $P\bar{1}$ with a *syn* disposition of the MeNC ligands, while **12** and **13** both occur on an inversion center in space group $P\bar{1}$, which demands an *anti* configuration of the two MeNC ligands. An upshot of the *syn* configuration in **11** is an intermetal distance that is ~1.3 Å shorter than that in **12** and

Table 3. Selected Interatomic Distances (Å) and Angles (deg) for 8

Ni···Ni	2.8406(9)
Ni–N	1.941[3]
Ni–$S_{nonbridging}$	2.1508[10]
Ni–$S_{bridging,\ cis\ to\ N}$	2.2158[10]
Ni–$S_{bridging,\ trans\ to\ N}$	2.1411[9]
Ni–S_{br}–Ni	81.36[3]
S_{br}–Ni–S_{br}	80.68[4]
S–Ni–S_{trans}	167.33[4]
S–Ni–$S_{chelate}$	89.72[4]
N–Ni–$S_{br,\ trans}$	174.09[9]
φ^a (deg)	74.3
τ^b (deg)	62.8

[a]Angle between $(C_2S_2)Ni$ coordination planes. [b]Fold angle between Ni–S_{br}–Ni planes.

https://dx.doi.org/10.1021/acs.organomet.0c00375
Organometallics 2020, 39, 2854–2870

Table 4. Selected Interatomic Distances (Å) and Angles (deg) in Phosphine MeNC Complexes

	9	10	11	12	13
M−S[a]	2.1392(5)	2.1407(5)	2.1345[6][i]	2.2727(9)	2.2780(10)
M−S[b]	2.1602(5)	2.1497(5)	2.1463[6]	2.2851(9)	2.2901(10)
Δ_{M-S}	0.021	0.009	0.0118	0.0124	0.0121
M−P	2.1908(5)	2.2025(5)	2.2028[6]	2.3210(9)	2.2881(10)
M−CNMe	1.8213(18)	1.8233(19)	1.826[2]	1.982(4)	1.958(4)
C≡N	1.148(2)	1.155(3)	1.153[3]	1.138(5)	1.130(5)
S−M−S	91.045(18)	90.780(19)	90.57[2]	88.00(3)	88.02(3)
C−M−P	90.72(6)	93.36(6)	91.16[6]	92.15(10)	90.62(11)
S−M−CNMe[c]	177.74(6)	167.92(6)	177.85[7]	176.20(10)	177.18(11)
S−M−P[c]	89.737(19)	90.576(19)	90.76[2]	91.46(3)	91.66(3)
S−M−CNMe[d]	88.78(6)	88.06(6)	87.54[6]	88.53(10)	89.86(11)
S−M−P[d]	172.788(19)	166.47(2)	177.07[3]	174.31(3)	174.95(3)
δ^e (Å)	0.078	0.187	0.010, 0.047	0.062	0.059
τ^f (Å)			7.848	9.138	9.162
θ^g (deg)	7.5	17.7	1.1, 4.9	5.7	5.4
φ^h (deg)			67.4	0.0	0.0

[a]S atom *trans* to MeNC. [b]S atom *trans* to phosphorus. [c]Angle defined with S atom *trans* to MeNC. [d]Angle defined with S atom *cis* to MeNC. [e]Average atom displacement from MS_2CP mean plane. [f]Distance between M atoms. [g]Angle between MS_2 and MPC planes. [h]Angle between the two MS_2PC planes at each end of the dimetallic molecule. [i]Brackets designate uncertainties propagated in averaging.

Table 5. Selected Interatomic Distances (Å) and Angles (deg) in CN^-, Carbene, and Ketenimine Complexes

	$[16]^-$	$[17]^-$	19	20[g]	21
M−S[a]	2.2605(7)	2.2716(7)	2.2697(14)	2.272[1]	2.1292(8)
M−S[b]	2.2821(7)	2.2908(7)	2.2808(13)	2.317[1]	2.1625(8)
Δ_{M-S}	0.0216	0.0192	0.0111	0.045	0.033
M−CN, M−$C_{carbene/ketenimine}$	2.019(2)	1.993(2)	2.046(5)	2.057[6]	1.906(3)
M−CNMe	1.996(2)	1.953(3)	1.997(6)	1.948[6]	1.830(3)
C≡NMe	1.131(3)	1.140(3)	1.127(7)	1.135[7]	1.148(4)
C−$C_{ketenimine}$				1.490[8]	
S−M−S	88.911(16)	88.858(18)	88.29(5)	88.86[5]	90.79(3)
C−M−C	92.50(7)	92.08(8)	92.9(5)	92.7[2]	89.47(13)
S−M−CNMe[c]	176.81(5)	177.86(7)	174.21(16)	178.3[2]	174.77(10)
S−M−CN[c]	177.78(6)	176.70(6)			
S−M−$C_{carbene/ketenimine}$[c]			179.59(15)	175.4[1]	175.96(9)
S−M−CNMe[d]	90.42(5)	90.97(6)	86.72(16)	90.9[1]	94.41(9)
S−M−CN[d]	88.22(5)	88.14(6)			
S−M−$C_{carbene/ketenimine}$[d]			92.09(14)	87.8[1]	85.32(9)
C−C−$N_{ketenimine}$				113.0[4]	
C−N−$CH_{3,ketenimine}$				118.1[5]	
δ^e (Å)	0.0267	0.0266	0.0252	0.0371, 0.0396	0.0064
θ^f (deg)	2.5	2.5	2.9	3.4, 3.7	1.2

[a]S atom *trans* to MeNC. [b]S atom *trans* to NC^- or carbene. [c]Angle defined with S atom *trans* to MeNC, NC^-, or carbene. [d]Angle defined with S atom *cis* to MeNC, CN^-, carbene, or ketenimine. [e]Average atom displacement from MS_2CP mean plane. [f]Angle between MS_2 and MC_2 planes. [g]Two independent molecules occur in the asymmetric unit. Values are averages of corresponding values from both molecules, and brackets designate uncertainties propagated in averaging.

13 (Table 4), while a consequence of the occurrence of **12** and **13** on inversion centers is a parallel disposition of the S_2MPC mean planes that contrasts with an angle of 67.4° for the square-planar ends in **11**.

Displacement of MeNC in $[(Ph_2C_2S_2)Ni(CNMe)_2]$ by CN^- can occur twice to afford $[(Ph_2C_2S_2)Ni(CN)_2]^{2-}$ $[\mathbf{15}]^{2-}$, but in poor yields of ∼9%. The same dianion, however, is accessible in ∼34% yield in the reaction between $[Ni(CN)_4]^{2-}$ and $[(Ph_2C_2S_2)Ni(CNMe)_2]$. With $[(Ph_2C_2S_2)M(CNMe)_2]$ (M = Pd^{2+}, Pt^{2+}), only monosubstitution to $[(Ph_2C_2S_2)M(CN)(CNMe)]^{1-}$ occurs (M = Pd^{2+}, $[\mathbf{16}]^-$; M = Pt^{2+}, $[\mathbf{17}]^-$), evidently because enhanced dipositive character for the second and third metals provides for stronger metal−ligand bonding. Although no appreciable difference in M−CNMe bond lengths exists between **5a** vs $[\mathbf{16}]^-$ or **6a** vs $[\mathbf{17}]^-$, the M−S bond lengths in $[\mathbf{16}]^-$ and $[\mathbf{17}]^-$ reveal a modest difference of ∼0.02 Å (Table 5) that suggests a slightly stronger *trans* influence for CN^- over CNMe.

Compounds **4a** and **5a** undergo substitution of CNMe by IPr (IPr = 1,3-bis(2,6-diisopropylphenyl)imidazol-2-ylidene) to afford $[(Ph_2C_2S_2)M(IPr)(CNMe)]$ (M = Ni^{2+}, **18**; M = Pd^{2+}, **19**), the structures of which reveal a difference of 0.011−0,020 Å between M−S bond lengths (Table 5). This difference is in accord with a documented ligand field strength for Arduengo-type carbene ligands that is at least comparable to that of phosphines and CN^-. Instead of simple ligand substitution, the reaction between **6a** and IPr leads unexpectedly to a ketenimine-type ligand formed by attach-

https://dx.doi.org/10.1021/acs.organomet.0c00375
Organometallics 2020, 39, 2854−2870

ment of the carbene carbon to the isonitrile carbon. The C–$C_{ketenimine}$ bond length of 1.490[8] Å, which is indicative of single-bond character, and an intraligand C–C–N angle of 113.0[4]°, which points toward sp^2 character for the carbon atom bound to Pt, are indicative of the charge-separated resonance form of the ketenimine (Scheme 6b) being the

Scheme 6. Resonance Forms of a Ketenimine

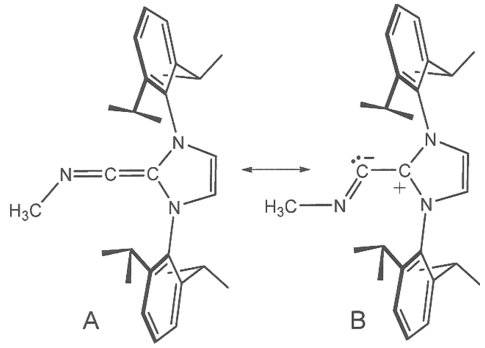

dominant contributor to its description. Insofar as Δ_{Pt-S} can be a gauge (Table 5), the ketenimine ligand appears to be an appreciably stronger field ligand than even the Arduengo carbene. We are not aware of any prior example of this type of ligand in this binding mode. As reported by Bielawski,[28] the free ketenimine that would be obtained by the reaction of C≡N-^{t}Bu and 1,3-bis(2,4,6-trimethylphenyl)imidazol-2-ylidene results in a similar angled geometry but faces unfavorable activation energetics. Carbene-derived ketenimines arising from a direct reaction between isocyanide and carbene only appear accessible from electronically perturbed carbene derivatives such as *N,N′*-diamido substituted variants.[28]

Use of tetraisopropylbenzobisimidazolium dibromide (Scheme 5), intended as a precursor to a bridging bis(carbene), in a reaction with **4a** produced an unanticipated Fischer carbene ligand wherein the carbenoid carbon is asymmetrically flanked by NMe_2 and NHMe groups. The probable genesis of this ligand is via condensation of a free C≡NMe molecule with bound C≡NMe, with hydrogen atoms possibly originating from an incompletely deprotected benzobisimidazolium dication or from adventitious moisture. In light of the well-documented capacity of carbenes to catalytically mediate a broad variety of carbon–carbon bond forming reactions,[29] this unanticipated outcome may involve the bis(carbene) complex activating either bound or free MeNC in a direct reaction, as opposed to accomplishing the intended straightforward substitution reaction. As gauged by the Δ_{M-S} values, the carbene ligand in **21** exerts a somewhat stronger *trans* influence than IPr, possibly because the larger steric profile of the latter tends to limit its bonding distance to M^{2+}. The asymmetry to the carbene ligand in **21** appears not to have a precedent, at least not in a structurally authenticated compound, but the symmetric noncyclic $C(NMe_2)_2$ carbene has been used in a few instances as a ligand in group 11 complexes.[30,31]

Spectroscopy. Compound sets **4–6** exhibit two infrared stretching frequencies in the 2100–2300 cm^{-1} region, which arise from the symmetric and antisymmetric vibrations of the C≡NR pair. These frequencies occur at *higher* energy in comparison to those found for the free isonitriles (Table 6), indicating that π back-bonding is not relevant to the metal–

Table 6. Summary of Infrared C≡N Stretching Frequencies (cm^{-1}) in CH_2Cl_2 Solution

	M = Ni	M = Pd	M = Pt
[(pdt)M(CNMe)$_2$][a] (2168)[b]	2228, 2214	2246, 2230	2248, 2223
[(pdt)M(CNBn)$_2$] (2155)[b]	2213, 2197	2227, 2213	2229, 2204
[(pdt)M(CNCy)$_2$] (2144)[b]	2204, 2189	2217, 2203	2219, 2196
[(pdt)M(CN^{t}Bu)$_2$] (2140)[b]	2197, 2180	2213, 2197	2214, 2188
[(pdt)M(CN-1-Ad)$_2$] (2133)[b]	2196, 2175	2211, 2198	2212, 2192
[(pdt)M(CNPh)$_2$] (2130)[b]	2182, 2162	2198, 2182	2199, 2172
[(adt)M(CN^{t}Bu)$_2$][c]	2196, 2180		
[(mdt)M(CN^{t}Bu)$_2$][d]	2196, 2177		
[(pdt)M(CN^{t}Bu)$_2$]$^+$			2243, 2222
[((pdt)M(CN^{t}Bu)$_2$)$_2$(μ-Ag)$_2$]$^{2+}$	2211, 2198		
[(pdt)M(CNMe)(PMe$_3$)]	2199		
[(pdt)M(CNMe)(PPh$_3$)]	2204		
[(pdt)M(CNMe)]$_2$(μ-1,4-dppb)	2223,[e] 2211	2240,[e] 2227	2237,[e] 2222
[(pdt)M(CN)$_2$]$^{2-}$	2100, 2095[f]		
[(pdt)M(CN)(CNMe)]$^-$		2227, 2120	2219, 2120
[(pdt)M(IPr)(CNMe)]	2190[f]	2213	
[(pdt)M(C(NMe)(IPr))(CNMe)]			2213
[(pdt)M(C(NMe)(IPr))(CNMe)]	2197		

[a]pdt = $[Ph_2C_2S_2]^{2-}$. [b]Value for free ligand. [c]adt = $[(CH_3O\text{-}p\text{-}C_6H_4)_2C_2S_2]^{2-}$. [d]mdt = $[(CH_3)_2C_2S_2]^{2-}$. [e]Shoulder. [f]Data have been previously published.

ligand interaction and suggesting instead that the increase in stretching frequency arises from an increased importance of resonance form A relative to B (Scheme 7) on ligation to

Scheme 7. Resonance Forms of an Isonitrile Ligand

metal. These stretching frequencies increase as one traverses the series from Ni^{2+} to Pd^{2+} to Pt^{2+} with a constant ligand, implying then an increasing positive character to the metal ion such that resonance form A is even further accentuated in its weighted contribution to the electronic description. A similar effect has been noted by Cotton in group 10 isocyanide complexes.[32] This behavior contrasts sharply with the 173–183 cm^{-1} shift to lower energy observed for ν_{CN} in the zerovalent homoleptic isocyanide compounds [M(CN(2,6-$Me_2C_6H_3$))$_6$] (M = V,[33] W[34]) and [M(CN(2,6-^{i}Pr$_2$C$_6$H$_3$))$_6$] (M = Nb,[35] Ta,[36] W[37]), in comparison to the free ligands. A decrease in ν_{CN} is found for **4–6** as R becomes more electron-donating (Me > Bn > Cy > ^{t}Bu ≈ 1-Ad), while Ph produces the lowest value for ν_{CN} through a presumed delocalizing effect upon the isocyanide π electrons.

Although π back-bonding does not describe the metal–isocyanide interaction in the compounds of Schemes 3 and 4, the isocyanide frequencies in [$(Ph_2C_2S_2)$M(CNMe)L] complexes manifest variation that apparently correlates to the σ donor power of L (Figure 2a). Stronger σ donors should moderate the positive character of M^{2+} and, because the negative end in charge-separated form A is then joined to the metal ion with attenuated cationic charge, they should tend to promote resonance form B over A. The shift from 2204 to 2199 and 2190 cm^{-1} for ν_{CN} in moving from [$(Ph_2C_2S_2)$Ni-

https://dx.doi.org/10.1021/acs.organomet.0c00375
Organometallics 2020, 39, 2854–2870

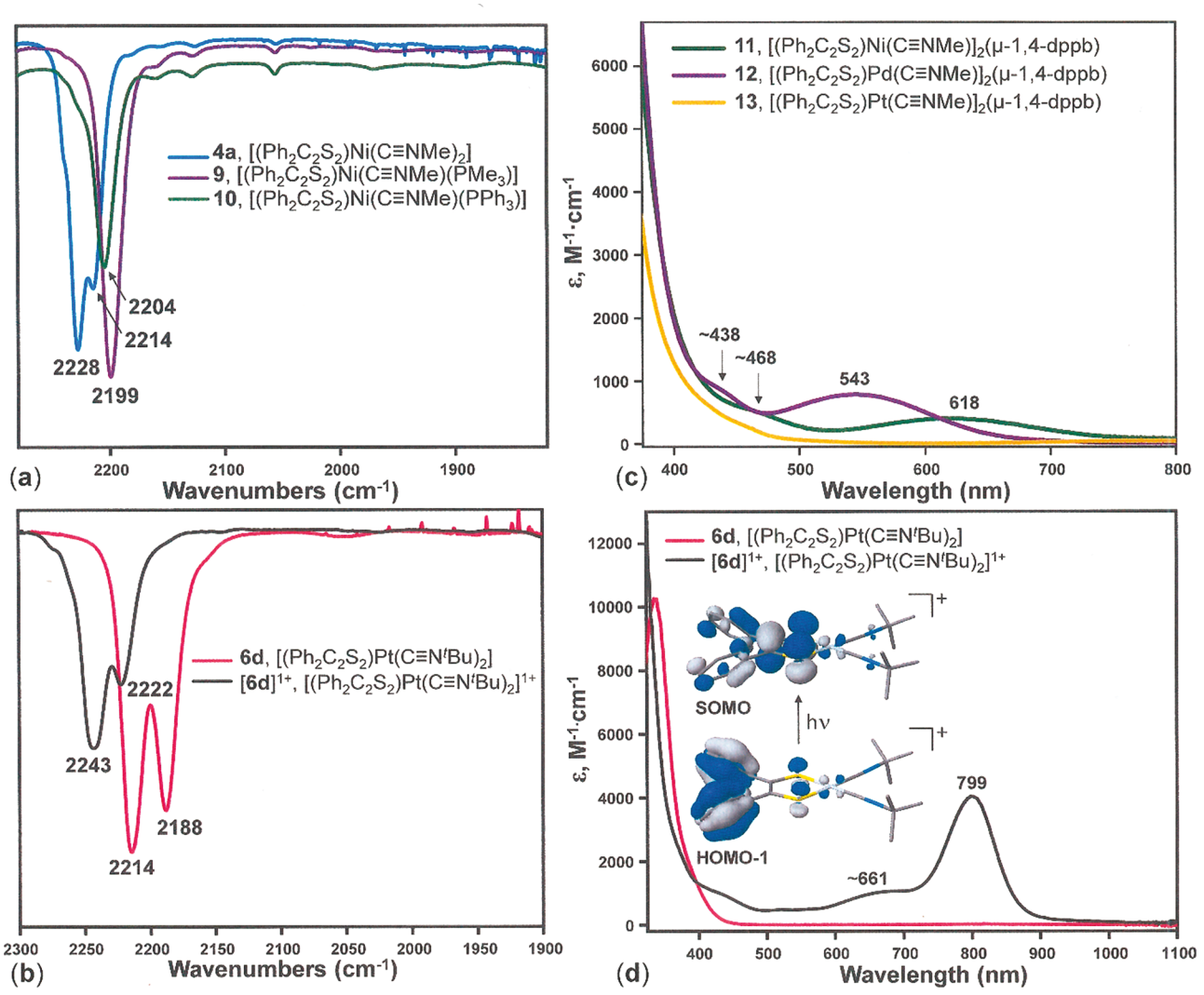

Figure 2. Selected IR (a, b) and UV−vis (c, d) spectra. The inset in (d) illustrates the MOs involved (0.04 contour level) with the 799 nm absorption.

$(CNMe)(PPh_3)]$ to $[(Ph_2C_2S_2)Ni(CNMe)(PMe_3)]$ and $[(Ph_2C_2S_2)Ni(CNMe)(IPr)]$ has a plausible basis in this light. In contrast, an effect of substantially greater magnitude is found for the $[(acac)Rh(CO)(PR_3)]$ series with R = Ph, Cy, Ad (ν_{CO} = 1977.6, 1958.7, 1948.3 cm^{-1}, respectively), where *bona fide* π back-bonding is likely operative.[38,39] For cationic $[(Ph_2C_2S_2)Pt(CN^tBu)_2]^+$ ($[\mathbf{6d}]^+$), both symmetric and antisymmetric ν_{CN} shift to higher energy by ~30 cm^{-1} (Table 6 and Figure 2b) due to an amplification of the positive character at Pt^{2+} by oxidation of the dithiolene ligand to a monoanion and enhancement of structure A in Scheme 7. Structurally, in keeping with this increase in ν_{CN}, $[\mathbf{6d}]_2^{2+}$ shows a decrease in its average C≡N bond length by ~0.014 Å relative to **6d** (Tables 1 and 2). A more modest increase in ν_{CN} by ~16 cm^{-1} is observed for $[((Ph_2C_2S_2)Ni(CN^tBu)_2)_2(\mu\text{-}Ag)_2]^{2+}$ vs $[(Ph_2C_2S_2)Ni(CN^tBu)_2]$ since the positive charge, being associated with the Ag^+ ions, is less directly transmitted to the group 10 metal.

The UV−vis spectra of compounds **4** feature low-intensity absorptions at ~600 nm and at 420−460 nm, the former of which is a transition between the HOMO, comprised of the dithiolene π system, and the LUMO, which is M−L σ^* in nature and involves the metal $d_{x^2-y^2}$ atomic orbital. This band shifts to higher energy when M = Pd (~500 nm) and M = Pt (unresolved from other features at still higher energy) owing to the inherently higher energies of the d orbitals of the heavier metals (Table 7). The same pattern is evident in the mono(isocyanide) compounds of the type $[(Ph_2C_2S_2)M(CNMe)L]$. As M varies from Ni to Pd and Pt in $[(Ph_2C_2S_2)M(CNMe)]_2(\mu\text{-}1,4\text{-dppb})$, for example, the lowest energy absorption similarly moves from 618 to 543 nm to a position unresolved from higher energy absorption above ~450 nm (Figure 2c).

Oxidation of **6d** by one electron induces a dark color and the onset of an intense low-energy maximum at ~799 nm with an unresolved shoulder at ~661 nm (Figure 2d). Absorptions in the lower energy 900−1100 nm region are conspicuously absent. The related cation, $[((^tBu\text{-}p\text{-}C_6H_4)_2C_2S_2)Pt(4,4'\text{-}^tBu_2\text{-}bipy)]^+$ (λ_{max} = 728 nm) has been shown by Wieghardt and coworkers to be in thermal equilibrium with the dimeric dication $[((^tBu\text{-}p\text{-}C_6H_4)_2C_2S_2)Pt(4,4'\text{-}^tBu_2\text{-}bipy)]_2^{2+}$ (λ_{max} = 1015 nm) and to be favored at ambient temperature.[25] Considering the fundamental similarity between $[((^tBu\text{-}p\text{-}C_6H_4)_2C_2S_2)Pt(4,4'\text{-}^tBu_2\text{-}bipy)]^+$ and $[(Ph_2C_2S_2)Pt(C{\equiv}N^tBu)_2]^+$, the lack of any absorption feature at an energy lower than 800 nm suggests that $[(Ph_2C_2S_2)Pt(C{\equiv}N^tBu)_2]^+$ is the dominant

https://dx.doi.org/10.1021/acs.organomet.0c00375
Organometallics 2020, 39, 2854−2870

Table 7. Summary of UV−Vis Spectral Data for All Compounds

compound	electronic spectra, λ_{max}, nm (ε_M, M^{-1} cm^{-1})
$[(Ph_2C_2S_2)Ni(CNMe)_2]$[a]	274 (31700), 348 (17200), 445 (240), 604 (300)
$[(Ph_2C_2S_2)Ni(CNBn)_2]$	460 (400), 608 (420)
$[(Ph_2C_2S_2)Ni(CNCy)_2]$	440 (240), 601 (420)
$[(Ph_2C_2S_2)Ni(CN^tBu)_2]$	424 (260), 600 (410)
$[(MeO\text{-}p\text{-}C_6H_4)_2C_2S_2)Ni(CN^tBu)_2]$	420 (200), 607 (320)
$[(Me_2C_2S_2)Ni(CN^tBu)_2]$	350 (6400), 450 (290), 614 (170)
$[(Ph_2C_2S_2)Ni(CN\text{-}1\text{-}Ad)_2]$	437 (180), 599 (360)
$[(Ph_2C_2S_2)Ni(CNPh)_2]$	466 (1400), 639 (480)
$[(Ph_2C_2S_2)Pd(CNMe)_2]$	421 (690), 502 (530)
$[(Ph_2C_2S_2)Pd(CNBn)_2]$	427 (150), 518 (50)
$[(Ph_2C_2S_2)Pd(CNCy)_2]$	431 (430), 504 (490)
$[(Ph_2C_2S_2)Pd(CN^tBu)_2]$[a]	240 (32500), 336 (17300), 419 (860), 498 (620)
$[(Ph_2C_2S_2)Pd(CN\text{-}1\text{-}Ad)_2]$	430 (320), 505 (420).
$[(Ph_2C_2S_2)Pd(CNPh)_2]$	385 (5180), 534 (770)
$[(Ph_2C_2S_2)Pt(CNMe)_2]$	337 (4780)
$[(Ph_2C_2S_2)Pt(CNBn)_2]$	342 (1560)
$[(Ph_2C_2S_2)Pt(CNCy)_2]$	336 (9970)
$[(Ph_2C_2S_2)Pt(CN^tBu)_2]$	336 (10290)
$[(Ph_2C_2S_2)Pt(CN\text{-}1\text{-}Ad)_2]$	336 (6850)
$[(Ph_2C_2S_2)Pt(CNPh)_2]$[a]	274 (35800), 390 (4070)
$[(Ph_2C_2S_2)Pt(CN^tBu)_2]^+$	439 (910), 661 (1030), 799 (4050)
$[((Ph_2C_2S_2)Ni(CN^tBu)_2)_2(\mu\text{-}Ag)_2]^{2+}$	523 (~35)
$[(2,6\text{-}Me_2py)Ni(\mu_2\text{-}\eta^1,\eta^1\text{-}S',\eta^1\text{-}S''\text{-}S_2C_2Ph_2)]_2$	272 (8670), 364 (2800), 482 (2230), 693 (260)
$[((Ph_2C_2S_2)Ni(C{\equiv}NMe))_2(\mu\text{-}dppb)]$	468 (520), 618 (420)
$[((Ph_2C_2S_2)Pd(C{\equiv}NMe))_2(\mu\text{-}dppb)]$	438 (890), 543 (820)
$[((Ph_2C_2S_2)Pt(C{\equiv}NMe))_2(\mu\text{-}dppb)]$	340 (11800)
$[(Ph_2C_2S_2)Ni(CNMe)(PMe_3)]$	564 (370)
$[(Ph_2C_2S_2)Ni(CNMe)(PPh_3)]$	348 (3900), 463 (210), 622 (190)
$[(Ph_2C_2S_2)Ni(CN)_2]^{2-}$	489 (220), 378 (5380)
$[(Ph_2C_2S_2)Pd(CN)(CNMe)]^{1-}$	338 (9800), 553 (920)
$[(Ph_2C_2S_2)Pt(CN)(CNMe)]^{1-}$	497 (1350)
$[(Ph_2C_2S_2)Ni(IPr)(CNMe)]$[a]	350 (11600), 560 (410), 867 (120)
$[(Ph_2C_2S_2)Pd(IPr)(CNMe)]$	470 (370)
$[(Ph_2C_2S_2)Pt(C(NMe)(IPr))(CNMe)]$	344 (7530)
$[(Ph_2C_2S_2)N(CNMe)(C(NHMe)(NMe_2))]$	510 (200)

[a]Data have been previously published.

species in solution and that $[[(Ph_2C_2S_2)Pt(C{\equiv}N^tBu)_2]_2]^{2+}$, although the form identified in the crystalline state, has a negligible concentration in CH_2Cl_2 at 25 °C. Time-dependent DFT calculations on $[(Ph_2C_2S_2)Pt(C{\equiv}N^tBu)_2]^+$ suggest that the 799 nm absorption is due to an intraligand dithiolene π (phenyl) → π (C_2S_2) excitation ((Figure 2d, inset) and that the 661 nm band is similar in description but involves the HOMO-2 with a different constitution to its phenyl π character.

The one-electron oxidation generally observed for compound types **4**−**6** is predominantly based on the C_2S_2 π system of the dithiolene ligand and produces a delocalized radical monoanion that gives rise to an isotropic signal. The *g* value for this signal is subject to minor variation as a function of the nature of the isocyanide substituent R (Figure 3). A slight shift to higher *g* values is found as R varies from Me to the more

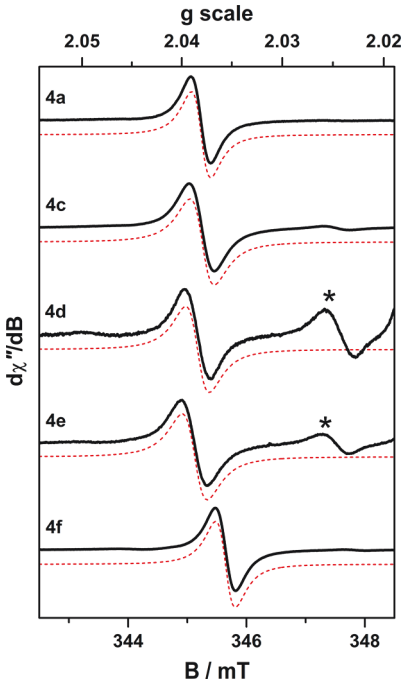

Figure 3. Comparison of the X-band EPR spectra of one-electron-oxidized **4a,c**−**f** recorded in CH_2Cl_2 solution at 293 K (experimental conditions: frequency, 9.808 GHz; power, 6.3 mW; modulation, 0.5 mT). Experimental data are represented by the black line, and simulation is depicted by the dashed trace: $[\mathbf{4a}]^+$, g_{iso} = 2.0381; $[\mathbf{4c}]^+$, g_{iso} = 2.0383; $[\mathbf{4d}]^+$, g_{iso} = 2.0386; $[\mathbf{4e}]^+$, g_{iso} = 2.0386; $[\mathbf{4f}]^+$, g_{iso} = 2.0353. The asterisk denotes an impurity caused by partial decomposition of the oxidized species at ambient temperature.

electron-rich ^{t}Bu and 1-adamantyl, while a somewhat greater move to lower *g* value is observed when R = Ph. As noted earlier in the context of C≡N stretching frequencies, the Ph π system exerts a modest delocalizing influence upon the C≡N multiple bond; indirectly therefrom, the Ph group registers more effect upon the dithiolene radical than its aliphatic counterparts.

Electrochemistry. Compound sets **4**−**6** display a reversible or quasi-reversible one-electron oxidation that is due to the $Ph_2C_2S_2^{2-}$ → $Ph_2C_2S^{-}S^{\bullet}$ + e^- transformation. Consistent with the increasing positive character at metal that is indicated by ν_{CN} stretching frequencies (*vide supra*), the potentials for these oxidations (E_{ox}) trend toward more positive values as M varies from Ni to Pd and Pt (Table 8). Where available, data for $[(Ph_2C_2S_2)M(CNMe)L]$ (L = phosphine, carbene) show E_{ox} values that move toward less positive values as the donor strength of L increases and renders the oxidation more facile. Thus, E_{ox} values for $[(Ph_2C_2S_2)Ni(CNMe)]_2(\mu$-1,4-dppb), $[(Ph_2C_2S_2)Ni(CNMe)(IPr)]$, and $[(Ph_2C_2S_2)Ni(CNMe)(C(NHMe)(NMe_2)]$ trend as +0.51 V > +0.41 V > +0.35, respectively. The basicity of the noncyclic carbene in **21** is likely greater than that of IPr in **18** because of a delocalizing effect of the imidazole ring in the latter. The electrochemistry of dimetallic compounds **11**−**13** is essentially similar to that of monometallic congeners **9** and **10** because their redox-active $M(S_2C_2Ph_2)$ end groups are far enough apart so as to be effectively independent. Thus, the waves they reveal at +0.51−0.57 V are attributed to concurrent one-electron oxidations of

https://dx.doi.org/10.1021/acs.organomet.0c00375
Organometallics 2020, 39, 2854−2870

Table 8. Summary of Cyclic Voltammetry Data (V) for $[(pdt)M(L_1)(L_2)]$ in CH_2Cl_2 with $[^nBu_4N][PF_6]$ Supporting Electrolyte[a]

L_1	L_2	M = Ni	M = Pd	M = Pt
MeNC	MeNC	+0.52	+0.61	+0.64
$C_6H_5CH_2NC$	$C_6H_5CH_2NC$	+0.50	+0.56	+0.57
CyNC	CyNC	+0.56	+0.61	+0.67
^{t}BuNC	^{t}BuNC	+0.59	+0.60	+0.66
^{t}BuNC	^{t}BuNC	+0.50[b]		
^{t}BuNC	^{t}BuNC	+0.42[c]		
1-Ad-NC	1-Ad-NC	+0.57	+0.59	+0.65
PhNC	PhNC	+0.62	+0.67	+0.73
2,6-Me_2py	μ_2-S-C_2Ph_2S	+0.05, +0.67[d]		
MeNC	1,4-$(Ph_2P)_2C_6H_4$	+0.51, +1.26[e]	+0.52, +0.93[d]	+0.57, +1.26[d]
CN^{1-}	CN^{1-}	−0.07		
MeNC	CN^{1-}		+0.27	+0.26
MeNC	IPr	+0.41, +1.78[e]	+0.33	
MeNC	C(NMe)IPr			+0.28
MeNC	C(NHMe)(NMe$_2$)	+0.35		

[a]All waves are reversible except where noted otherwise. Potentials are referenced with respect to AgCl/Ag. Under these conditions, the Cp_2Fe^+/Cp_2Fe couple consistently occurred at +540 mV. [b]The dithiolene ligand is $[(CH_3O\text{-}p\text{-}C_6H_4)_2C_2S_2]^{2-}$ rather than $[Ph_2C_2S_2]^{2-}$. [c]The dithiolene ligand is $[Me_2C_2S_2]^{2-}$ rather than $[Ph_2C_2S_2]^{2-}$. [d]Quasi-reversible wave. [e]Irreversible wave.

the metallodithiolene end groups such that, as has been found for dimetallic compounds of the composition $[(R_2C_2S_2)M(\mu_2\text{-tpbz})M(S_2C_2R_2)]$[40,41] (tpbz = 1,2,4,5-tetrakis(diphenylphosphino)benzene), two remotely coupled radical monoanions are generated.

Compound **8** differs in kind from those of the type $[(Ph_2C_2S_2)M(CNMe)L]$ in having no MeNC ligands. More importantly, while the compound is dimetallic, the bridging interactions are provided by a thiolate sulfur atom from each of the two dithiolene ligands. Consequently, the $Ni_2(\mu_2\text{-}\eta^1,\eta^1\text{-}S',\eta^1\text{-}S''\text{-}C_2S_2Ph_2)_2$ core can only be regarded as a single redox-active entity rather than as two independent fragments as in **11**−**13**. The cyclic voltammogram of **8** shows a reversible wave at +0.05 V, substantially less positive by ∼+0.50 V than the oxidations found for compounds **4**. This feature is followed by a quasi-reversible oxidation at +0.67 V (Figure 4). As suggested by symmetry considerations and by its relatively compact core, the HOMO for **8** is largely composed of the C_2S_2 π systems of the two identical dithiolene ligands with a modest contribution from Ni^{2+}. Delocalization of charge in $[\mathbf{8}]^+$ throughout the $Ni_2(\mu_2\text{-}\eta^1,\eta^1\text{-}S',\eta^1\text{-}S''\text{-}S_2C_2Ph_2)_2$ center enables both the milder oxidation potential for **8** and, most likely, its capacity to sustain another oxidation where compounds **4** cannot. Were it to be isolated, $[\mathbf{8}]^+$ is anticipated to show $C\text{−}C_{chelate}$ and S−C bond lengths between those of the fully reduced ene-1,2-dithiolate and the radical monoanion (Scheme 1a,b, respectively) since the presumed one-electron oxidation is averaged over two ligands. The LUMO for **8** is calculated as being ∼2.8 eV higher in energy than the HOMO and, similar to compounds **4**−**6**, is M $(d_{x^2-y^2})$−L (σ^*) in nature.

Summary. The principal findings of this work are as follows.

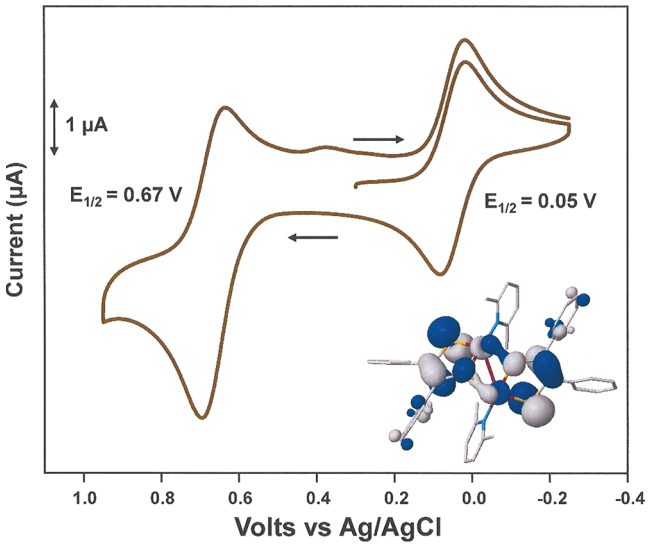

Figure 4. Cyclic voltammogram of $[(2,6\text{-}Me_2py)Ni(\mu_2\text{-}\eta^1,\eta^1\text{-}S',\eta^1\text{-}S''\text{-}S_2C_2Ph_2)]_2$ in CH_2Cl_2 with $[Bu_4N][PF_6]$ supporting electrolyte. The figure inset illustrates the HOMO (0.03 contour level), which is largely comprised of the C_2S_2 portions of the dithiolene ligands.

(1) The syntheses of $[(Ph_2C_2S_2)M(C{\equiv}NR)_2]$ (M = Ni^{2+}, Pd^{2+}, Pt^{2+}; R = Me, Bn, Cy, ^{t}Bu, 1-adamantyl, Ph) proceed by dithiolene substitution from homoleptic $[(Ph_2C_2S_2)_2M]$. All compounds are air-stable and are amenable to purification by column chromatography. Yields of isolated material are in the ranges 72−91% for M = Ni^{2+}, 55−80% for M = Pd^{2+}, and 37−52% for M = Pt^{2+}, implying stronger metal−dithiolene binding in moving from the first-row to the third-row metal.

(2) Between this report and a preceding communication, all 18 members of the set have been characterized by X-ray crystallography. Progressively greater square planarity is observed in moving from Ni^{2+} to Pd^{2+} and Pt^{2+}.

(3) The ν_{CN} stretching frequencies in $[(Ph_2C_2S_2)M(C{\equiv}NR)_2]$ all occur at higher energy in comparison to the free ligand and increase in energy as M varies from Ni^{2+} to Pd^{2+} and Pt^{2+}. This trend is rationalized as arising from increasing cationic character for the heavier metals, which tends to promote the linear, charge-separated resonance form of the isonitrile ligand ($:C^-{\equiv}N^+{-}R$) over its bent counterpart ($:C{=}\ddot{N}{-}R$).

(4) Compound types $[(Ph_2C_2S_2)M(C{\equiv}NR)_2]$ and $[(Ph_2C_2S_2)M(C{\equiv}NR)L]$ sustain a reversible or quasi-reversible one-electron oxidation due to the redox-active dithiolene ligand: $Ph_2C_2S_2^{2-} - e^- \rightarrow Ph_2C_2S^-S^\bullet$. In the case of $[(Ph_2C_2S_2)Pt(C{\equiv}N^tBu)_2]$, treatment with $[(Br\text{-}p\text{-}C_6H_4)_3N][SbCl_6]$ and crystallization of the isolated product yields centrosymmetric dimeric $[[(Ph_2C_2S_2)Pt(C{\equiv}N^tBu)_2]_2]^{2+}$ formed via Pt···S axial interactions in a rhombic $(Pt{\cdots}S)_2$ core.

(5) The $[(Ph_2C_2S_2)M(C{\equiv}NMe)_2]$ compounds provide access to new heteroleptic dithiolene compounds by displacement of MeN≡C with various other ligands (CN^-, phosphine, carbene). The spectroscopic and electrochemical properties of $[(Ph_2C_2S_2)M(C{\equiv}NMe)L]$ trend according to the σ-donor strength of L.

(6) Differences as a function of M in the pattern of MeN≡C displacement from $[(Ph_2C_2S_2)M(C{\equiv}NMe)_2]$ arise from strengthened M−C≡NMe binding in moving

https://dx.doi.org/10.1021/acs.organomet.0c00375
Organometallics 2020, 39, 2854−2870

from M = Ni^{2+} to Pd^{2+} and Pt^{2+}. Thus, for M = Ni^{2+} and Pd^{2+}, the Arduengo carbene IPr reacts with $[(Ph_2C_2S_2)M(C{\equiv}NMe)_2]$ to form $[(Ph_2C_2S_2)M(IPr)(C{\equiv}NMe)]$, while for $[(Ph_2C_2S_2)Pt(C{\equiv}NMe)_2]$, IPr attacks the isocyanide carbon to form an $\eta^1,\kappa C$-ketenimine ligand in a bent, charge-separated resonance form.

In continuing work, we are probing the utility of $[(Ph_2C_2S_2)M(C{\equiv}NMe)_2]$ as synthons toward new metallodithiolene compounds, including multimetallic compounds, that are not accessible by other routes.

■ ASSOCIATED CONTENT

Supporting Information

The Supporting Information is available free of charge at https://pubs.acs.org/doi/10.1021/acs.organomet.0c00375.

Procedures for crystal growth, X-ray diffraction data collection, and structure solution and refinement, summary of unit cell and refinement data, thermal ellipsoid plots with complete atom labeling, spectroscopic, electrochemical, and analytical data for the compounds reported, and description of computation procedures (PDF)

Coordinates for geometry optimized structures (XYZ)

Accession Codes

CCDC 1920776−1920790 and 1995894−1995907 contain the supplementary crystallographic data for this paper. These data can be obtained free of charge via www.ccdc.cam.ac.uk/data_request/cif, or by emailing data_request@ccdc.cam.ac.uk, or by contacting The Cambridge Crystallographic Data Centre, 12 Union Road, Cambridge CB2 1EZ, UK; fax: +44 1223 336033.

■ AUTHOR INFORMATION

Corresponding Author

James P. Donahue − *Department of Chemistry, Tulane University, New Orleans, Louisiana 70118-5698, United States;* orcid.org/0000-0001-9768-4813; Email: donahue@tulane.edu

Authors

Antony Obanda − *Department of Chemistry, Tulane University, New Orleans, Louisiana 70118-5698, United States;* orcid.org/0000-0003-3532-0402

Kendra Valerius − *Department of Chemistry, Tulane University, New Orleans, Louisiana 70118-5698, United States*

Joel T. Mague − *Department of Chemistry, Tulane University, New Orleans, Louisiana 70118-5698, United States*

Stephen Sproules − *WestCHEM, School of Chemistry, University of Glasgow, Glasgow G12 8QQ, United Kingdom;* orcid.org/0000-0003-3587-0375

Complete contact information is available at: https://pubs.acs.org/10.1021/acs.organomet.0c00375

Notes

The authors declare no competing financial interest.

■ ACKNOWLEDGMENTS

The Louisiana Board of Regents (LEQSF-(2002-03)-ENH-TR-67) and the National Science Foundation (MRI: 1228232 and 0619770) are thanked for funding of Tulane University's X-ray crystallography and mass spectrometry instrumentation, and Tulane University is acknowledged for its ongoing assistance with operational costs for the X-ray diffraction facility. A.O. and J.P.D. gratefully acknowledge support for this project from the National Science Foundation (CHE: 1836589). Ms. Titir Das Gupta is thanked for assistance with addressing a few experimental measurements.

■ REFERENCES

(1) Schrauzer, G. N.; Mayveg, V. P.; Heinrich, W. Coordination Compounds with Delocalized Ground States. α-Dithiodiketone-Substituted Group VI Metal Carbonyls and Related Compounds. *J. Am. Chem. Soc.* **1966**, *88*, 5174−5179.

(2) Enemark, J. H.; Cooney, J. J. A.; Wang, J.-J.; Holm, R. H. Synthetic Analogues and Reaction Systems Relevant to the Molybdenum and Tungsten Oxotransferases. *Chem. Rev.* **2004**, *104*, 1175−1200.

(3) Nomura, M.; Okuyama, R.; Fujita-Takayama, C.; Kajitani, M. New Synthetic Methods for η^5-Cyclopentadienyl Nickel(III) Dithiolene Complexes Derived from Nickelocene. *Organometallics* **2005**, *24*, 5110−5115.

(4) Adams, H.; Morris, M. J.; Morris, S. A.; Motley, J. C. Dithiolene Transfer from Nickel to a Dimolybdenum Centre: the First Dithiolene Alkyne Complex. *J. Organomet. Chem.* **2004**, *689*, 522−527.

(5) Adams, H.; Gardner, H. C.; McRoy, R. A.; Morris, M. J.; Motley, J. C.; Torker, S. Heterometallic Dithiolene Complexes Formed by Stepwise Displacement of Cyclopentadienyl Ligands from Nickelocene with $CpMo(S_2C_2Ph_2)_2$. *Inorg. Chem.* **2006**, *45*, 10967−10975.

(6) Adams, H.; Coffey, A. M.; Morris, M. J.; Morris, S. A. Efficient Transfer of Either One or Two Dithiolene Ligands from Nickel to Ruthenium: Synthesis and Crystal Structures of $[Ru(SCR{=}CPhS)_2(PPh_3)]$ and $[RuCl_2(SCR{=}CPhS)(PPh_3)_2]$ (R=Ph, H). *Inorg. Chem.* **2009**, *48*, 11945−11953.

(7) Adams, H.; Grimes, L.; Morris, M. J.; Robertson, C. C. Dithiolene Transfer to the Molybdenum Nitrosyl Complex $[CpMo(CO)_2(NO)]$: Formation of Bimetallic Complexes. *J. Organomet. Chem.* **2018**, *877*, 73−79.

(8) Adams, H.; Morris, M. J.; Robertson, C. C.; Tunnicliffe, H. C. I. Synthesis of Mono- and Diiron Dithiolene Complexes as Hydrogenase Models by Dithiolene Transfer Reactions, Including the Crystal Structure of $[\{Ni(S_2C_2Ph_2)\}_6]$. *Organometallics* **2019**, *38*, 665−676.

(9) Mayweg, V. P.; Schrauzer, G. N. Bis-adducts of Group VIII Metal Bisdithiobenzil Complexes with Phosphines. *Chem. Commun.* **1966**, 640−641.

(10) Obanda, A.; Martinez, K.; Schmehl, R. H.; Mague, J. T.; Rubtsov, I. V.; Macmillan, S. N.; Lancaster, K. M.; Sproules, S.; Donahue, J. P. Expanding the Scope of Ligand Substitution from $[M(S_2C_2Ph_2)_2]$ (M = Ni^{2+}, Pd^{2+}, Pt^{2+}) to Afford New Heteroleptic Dithiolene Complexes. *Inorg. Chem.* **2017**, *56*, 10257−10267.

(11) Hanson, G. R.; Gates, K. E.; Noble, C. J.; Griffin, M.; Mitchell, A.; Benson, S. XSophe-Sophe-XeprView®. A Computer Simulation Software Suite (v. 1.1.3) for the Analysis of Continuous Wave EPR Spectra. *J. Inorg. Biochem.* **2004**, *98*, 903−916.

(12) Schuster, R. E.; Scott, J. E.; Casanova, J., Jr. Methyl Isocyanide. *Org. Synth.* **1966**, *46*, 75−77.

(13) Eckert, H.; Nestl, A.; Ugi, I. Phenylisonitrile. In *Encyclopedia of Reagents for Organic Synthesis*; Wiley: 2001.

(14) Gokel, G. W.; Widera, R. P.; Weber, W. P. Phase-Transfer Hofmann Carbylamine Reaction: *tert*-Butyl Isocyanide. *Org. Synth.* **1976**, *55*, 96−99.

(15) Schmidtendorf, M.; Pape, T.; Hahn, F. E. Molecular Rectangles from Platinum(II) and Bridging Dicarbene, Diisocyanide, and 4,4'-Bipyridine Ligands. *Dalton Trans.* **2013**, *42*, 16128−16141.

(16) Bantreil, X.; Nolan, S. P. Synthesis of *N*-Heterocyclic Carbene Ligands and Derived Ruthenium Olefin Metathesis Catalysts. *Nat. Protoc.* **2011**, *6*, 69−77.

(17) Baldwin, R. A.; Cheng, M. T. Arylenebis(Tertiary Phosphines) and − (Phosphinic Acids. *J. Org. Chem.* **1967**, *32*, 1572−1577.
(18) Amarego, W. L. F.; Perrin, D. D. *Purification of Laboratory Chemicals*, 4th ed.; Butterworth-Heinemann: Oxford, U.K., 2000.
(19) Connelly, N. G.; Geiger, W. E. Chemical Redox Agents for Organometallic Chemistry. *Chem. Rev.* **1996**, *96*, 877−910.
(20) Arumugam, K.; Shaw, M. C.; Chandrasekaran, P.; Villagrán, D.; Gray, T. G.; Mague, J. T.; Donahue, J. P. Synthesis, Structures and Properties of 1,2,4,5-Benzenetetrathiolate Linked Group 10 Metal Complexes. *Inorg. Chem.* **2009**, *48*, 10591−10607.
(21) Robertson, S. D.; Slawin, A. M. Z.; Woollins, J. D. Constructing Multimetallic Systems with the Naphthalene-1,8-bis(thiolato) Ligand. *Eur. J. Inorg. Chem.* **2007**, 247−253.
(22) Shin, R. Y. C.; Tan, G. K.; Koh, L. L.; Vittal, J. J.; Goh, L. Y.; Webster, R. D. Metallophilicity in Annular Ru_2M_2 Derivatives of $(HMB)Ru^{II}(tpdt)$ versus (Bis)-η^2-Dithiolate Bonding in Ru_2M Derivatives of $Cp^*Ru^{III}(tpdt)$ (HMB = η^6-C_6Me_6; Cp* = η^5-C_5Me_5; M = Cu^I, $Ag^{I,II}$, Au^I; tpdt = 3-thiapentane-1,5-dithiolate). *Organometallics* **2005**, *24*, 539−551.
(23) Yu, R.; Arumugam, K.; Manepalli, A.; Tran, Y.; Schmehl, R.; Jacobsen, H.; Donahue, J. P. Reversible, Electrochemically Controlled Binding of Phosphine to Iron and Cobalt Bis(dithiolene) Complexes. *Inorg. Chem.* **2007**, *46*, 5131−5133.
(24) Sproules, S.; Wieghardt, K. *o*-Dithiolene and *o*-aminothiolate chemistry of iron: Synthesis, structure and reactivity. *Coord. Chem. Rev.* **2010**, *254*, 1358−1382.
(25) Pap, J. S.; Benedito, F. L.; Bothe, E.; Bill, E.; DeBeer George, S.; Weyhermüller, T.; Wieghardt, K. Dimerization Processes of Square Planar $[Pt^{II}(^t bpy)(dithiolato^{\bullet})]^+$ Radicals. *Inorg. Chem.* **2007**, *46*, 4187−4196.
(26) Pop, F.; Branzea, D. G.; Cauchy, T.; Avarvari, N. Bimetallic Neutral Palladium(II) Bis(dithiolene) Complex: Unusueal Synthesis, Structural and Theoretical Study. *C. R. Chim.* **2012**, *15*, 904−910.
(27) Chandrasekaran, P.; Greene, A. F.; Lillich, K.; Capone, S.; Mague, J. T.; DeBeer, S.; Donahue, J. P. A Structural and Spectroscopic Investigation of Octahedral Platinum Bis(dithiolene)-phosphine Complexes: Platinum Dithiolene Internal Redox Chemistry Induced by Phosphine Association. *Inorg. Chem.* **2014**, *53*, 9192−9205.
(28) Hudnall, T. W.; Moorhead, E. J.; Gusev, D. G.; Bielawski, C. W. *N,N'*-Diamidoketenimines via Coupling of Isocyanides to an *N*-Heterocyclic Carbene. *J. Org. Chem.* **2010**, *75*, 2763−2766.
(29) Enders, D.; Niemeier, O.; Henseler, A. Organocatalysis by N-Heterocyclic Carbenes. *Chem. Rev.* **2007**, *107*, 5606−5655.
(30) Coyle, J. P.; Sirianni, E. R.; Korobkov, I.; Yap, G. P. A.; Dey, G.; Barry, S. T. Study of Monomeric Copper Complexes Supported by *N*-Heterocyclic and Acyclic Diamino Carbenes. *Organometallics* **2017**, *36*, 2800−2810.
(31) Holthoff, J. M.; Engelage, E.; Kowsari, A. B.; Huber, S. M.; Weiss, R. Noble Metal Corrosion: Halogen Bonded Iodocarbenium Iodides Dissolve Elemental Gold − Direct Access to Gold-Carbene Complexes. *Chem. - Eur. J.* **2019**, *25*, 7480−7484.
(32) Cotton, F. A.; Zingales, F. The Donor-Acceptor Properties of Isonitriles as Estimated by Infrared Study. *J. Am. Chem. Soc.* **1961**, *83*, 351−355.
(33) Barybin, M. V.; Young, V. G., Jr.; Ellis, J. E. First Paramagnetic Zerovalent Transition Metal Isocyanides. Syntheses, Structural Characterizations, and Magnetic Properties of Novel Low-Valent Isocyanide Complexes of Vanadium. *J. Am. Chem. Soc.* **2000**, *122*, 4678−4691.
(34) Lockwood, M. A.; Fanwick, P. E.; Rothwell, I. P. Reactivity of a Tungsten(II) Aryloxide with Isocyanides and Isocyanates. *Organometallics* **1997**, *16*, 3574−3575.
(35) Kucera, B. E.; Roberts, C. J.; Young, V. G., Jr.; Brennessel, W. W.; Ellis, J. E. Niobium Isocyanide Complexes, $Nb(CNAr)_6$, with Ar = 2,6-Dimethylphenyl (Xyl), a Diamagnetic Dimer Containing Four Reductively Coupled Isocyanides, and Ar = 2,6-Diisopropylphenyl (Dipp), a Paramagetic Monomer Analogous to the Highly Unstable Hexacarbonylniobium(0). *Acta Crystallogr., Sect. C: Struct. Chem.* **2019**, *75*, 1259−1265.
(36) Chakarawet, K.; Davis-Gilbert, Z. W.; Harstad, S. R.; Young, V. G., Jr.; Long, J. R.; Ellis, J. E. $Ta(CNDipp)_6$: An Isocyanide Analogue of Hexacarbonyltantalum(0). *Angew. Chem., Int. Ed.* **2017**, *56*, 10577−10581.
(37) Sattler, W.; Ener, M. E.; Blakemore, J. D.; Rachford, A. A.; LaBeaume, P. J.; Thackeray, J. W.; Cameron, J. F.; Winkler, J. R.; Gray, H. B. Generation of Powerful Tungsten Reductants by Visible Light Excitation. *J. Am. Chem. Soc.* **2013**, *135*, 10614−10617.
(38) Brink, A.; Roodt, A.; Steyl, G.; Visser, H. G. Steric *vs.* electronic anomaly observed from iodomethane oxidative addition to tertiary phosphine modified rhodium(I) acetylacetonato complexes following progressive phenyl replacement by cyclohexyl [PR_3 = PPh_3, PPh_2Cy, $PPhCy_2$, PCy_3]. *Dalton Trans.* **2010**, *39*, 5572−5578.
(39) Chen, L.; Ren, P.; Carrow, B. P. Tri(1-adamantyl)phosphine: Expanding the Boundary of Electron-Releasing Character Available to Organophosphorus Compounds. *J. Am. Chem. Soc.* **2016**, *138*, 6392−6395.
(40) Arumugam, K.; Shaw, M. C.; Mague, J. T.; Bill, E.; Sproules, S.; Donahue, J. P. Long-Range Spin Coupling: A Tetraphosphine-Bridged Palladium Dimer. *Inorg. Chem.* **2011**, *50*, 2995−3002.
(41) Arumugam, K.; Selvachandran, M.; Obanda, A.; Shaw, M. C.; Chandrasekaran, P.; Caston Good, S. L.; Mague, J. T.; Sproules, S.; Donahue, J. P. Redox-Active Metallodithiolene Groups Separated by Insulating Tetraphosphinobenzene Spacers. *Inorg. Chem.* **2018**, *57*, 4023−4038.

https://dx.doi.org/10.1021/acs.organomet.0c00375
Organometallics 2020, 39, 2854−2870